Geomechanical, petrophysical, and mineralogical properties of limestone samples from Kansas

by

Nelsy Osorio

B.S., University of New Orleans, 2019

A THESIS

submitted in partial fulfillment of the requirements for the degree

MASTER OF SCIENCE

Department of Geology
College of Arts and Sciences

KANSAS STATE UNIVERSITY
Manhattan, Kansas

2025

Approved by:

Co-Major Professor
Dr. Brice LaCroix

Approved by:

Co-Major Professor
Dr. Behzad Ghanbarian

Copyright

Abstract

The use of limestone in aggregate production and infrastructure projects necessitates a comprehensive investigation of its geomechanical and mineralogical properties across various scales and conditions. This study investigates the geomechanical properties, specifically Young's Modulus E, in core and aggregate limestone samples from Kansas through the investigation and assessment of mineralogical and petrophysical variables. The main objectives of this study were to: (1) assess E in relation to mineralogical, petrophysical, and scale-dependent variability in Kansas limestone and (2) develop predictive models for E. For these purposes, we collected 29 1-inch and 28 2-inch limestone samples and measured E using uniaxial experiments under dry and saturated conditions. We present regression-based models in combination with decision trees that allow for the estimation of E based on water content θ and quartz content for saturated limestone samples. By comprehensively examining the geomechanical, petrophysical, and mineralogical properties of Kansas limestone cores, this study facilitates their utilization and suitability as aggregates in concrete production and various construction applications for the Kansas Department of Transportation (KDOT).

Table of Contents

List of Figures

List of Tables

Acknowledgements

I would like to sincerely thank my major professor, Dr. Behzad Ghanbarian. Your expertise, thoughtful guidance, and mentorship have been invaluable throughout the course of this work. You have greatly shaped my development as a researcher and scientist.

A special thanks to Dr. Brice LaCroix, my co-major advisor, for providing insight and assistance throughout this work. I thank Dr. Christopher Jones for serving on my committee and providing laboratory resources and support. I am thankful to have been provided the opportunity to learn invaluable skills in both of your laboratories. I gratefully acknowledge the Kansas Department of Transportation for their funding and collaboration throughout this project. I thank Dr. Subodh Mhamankar and all who provided laboratory assistance and support.

I thank the Department of Geology at Kansas State University and all the dedicated educators for providing an excellent learning environment.

To my friends and fellow students, thank you for your friendship and making my time here memorable.

I am grateful to Justin for being by my side with encouragement and love. Your support has made all the difference.

Lastly, I owe my deepest gratitude to my family for their unconditional love, support, and belief in me, which have sustained and inspired me. To my sisters, I cherish you deeply. You have made this journey possible.

Dedication

I dedicate this work to my beloved parents, Wendy and Leonel. This achievement is as much yours as it is mine.

Chapter 1 - Introduction

In Kansas, limestone is the predominant rock type and an abundant carbonate aggregate resource, with demand steadily increasing due to its durability and extensive use in concrete, road construction, and a variety of infrastructure projects. In 2024, natural aggregates led United States nonfuel mineral production, comprising 36% of the total value (U.S. Geological Survey, 2025), with limestone being one of the primary sources due to its high availability, mechanical strength, resistance to alkali-silica reaction, and reduced drying shrinkage in concrete (Aquino et al., 2010). Limestone aggregates that are susceptible to environmental degradation contribute to early pavement failure, reduced lifespan, and compromised safety and performance. Given the extensive use of limestones, identifying and predicting variables that influence their deformational behavior is essential to assessing key geomechanical properties, particularly Young's modulus E, a fundamental parameter used to study mechanical stability and material behavior under load (ASTM, 2017). E has broad applications in analyzing slope stability, rock failure criteria, reservoir characterization, materials science, hazard mitigation, and road and construction projects.

The geomechanical behavior of limestones is influenced by a variety of petrophysical and mineralogical properties. A comprehensive understanding of the relationships between E and key rock properties, including mineralogy and volumetric water content θ is essential for the characterization of limestone's geomechanical behavior. The influence of water on E has been widely investigated in the literature. For instance, Zhang et al. (2023) observed that E decreased with increasing water content, resulting in a 23.6% decrease even at low levels of saturation. Li et al. (2022) reported a strong negative correlation ($R^2 = 0.99$) between saturation time and E in jointed limestones, reporting a 68 % reduction in E after seven days. Wong et al. (2016) found that both *E* and strength decreased with increasing water content and noted exponential or power-law trends across multiple rock types. Limestone typically exhibited 30 to 40 % reductions in *E*, with some reductions reaching 60%. Sandstones experienced smaller losses in *E*, generally under 20%. In contrast, clay-rich rocks such as shale, siltstone, mudstone, and marl exhibited more severe reductions, with shale showing a mean *E* loss around 50% and some mudstones losing up to 90 to 100%. These reductions in geomechanical properties occur from a combination of physical and chemical mechanisms, both of which are influenced by mineralogy and water content. According to Li et al. (2022), crack density and crack length increased progressively with saturation time, leading to substantial mechanical degradation. They attributed this behavior to water gradually infiltrating pores and fissures, where it physically and chemically interacts with nearby hydrophilic minerals, and generates new joints and fissures. Similar weakening mechanisms include carbonate dissolution, quartz hydrolysis, increased pore pressure, reduced intergranular friction, and clay swelling (Cai et al, 2019). Overall, the literature indicates that clay-bearing rocks are particularly susceptible to these water-related weakening mechanisms. Erguler and Ulusay (2009) observed up to 93% reductions in *E* for rocks containing 15-81% clay, primarily swelling clays. Water weakens clay-bearing rocks through two main mechanisms, according to Liu et al. (2020). These consist of osmotic swelling within intergranular layer and the surface hydration of clay particles. For non-swelling clays, adsorbed water accumulates on the external surface of clay minerals. With increasing water, the mobility of this adsorbed film increases and enables slip between clay particles under pressure (Liu et al., 2020). Although water is widely known to reduce geomechanical properties, such as *E*, the joint contributions of mineralogy and water content remain uncertain.

Beyond water content, the mineralogical composition of limestone also exerts a strong influence on geomechanical behavior. Although calcite is typically the dominant mineral in limestone, the varying quantities of dolomite, quartz, and clay minerals in limestone can influence elastic properties. While high quartz content has been associated with increased stiffness, Wasantha et al. (2018) found that quartz alone did not control strength in sandstones and noted that grain size and porosity were also influential. Nonetheless, quartz appeared to reduce the extent of water-induced weakening, whereas sandstones with higher clay contents experienced more significant moduli reductions.

Among the common clay minerals in limestones, including illite, kaolinite, smectite, and chlorite, only smectite exhibits swelling. This behavior is characteristic of smectite, which expands when water or some polar organic compound, such as ethylene glycol, enters the interlayer space (Moore and Reynolds, 1989). The influence of clay minerals on elastic properties depends not only on the total clay content, but also on the types of clay and their distribution. For instance, sandstones with similar clay volumes may exhibit different elastic properties due to variation in clay types (Mondol et al., 2008). Furthermore, Vafaie and Kivi (2020) showed that among limestones with varying clay content, the argillaceous facies, characterized by elevated clay and organic matter, exhibited a lower E compared to the micritic limestone, which contains greater carbonate content.

Because direct laboratory measurements of E are time-consuming, destructive, and require well-prepared core samples (Ghafoori et al., 2018; Madhubabu, 2016), a variety of methods have been reported in the literature to estimate E. These methods include utilizing ultrasonic wave velocities, porosity-based regression models, artificial neural networks, effective medium and percolation models, and uniaxial compression testing (Aboutaleb et al., 2018;

Moradian and Behnia, 2009; Hadi and Nygaard, 2023; Osorio et al., 2025). Although studies have provided insights into the relationship between *E* and other rock properties, their findings are often limited to specific rock types, formations, depths, and geographic conditions, which limit their broad applicability.

Despite the extensive use of Kansas limestones in infrastructure, no studies have linked *E* to mineralogy and water content θ. Therefore, the present study aims to: (1) measure the geomechanical, petrophysical mineralogical properties of limestone samples from Kansas, (2) experimentally link *E* to θ, bulk mineralogy, and clay content across 1-inch and 2-inch core scales, and relate mineralogical composition across core and crushed aggregate scales, and (3) develop regression-based models for predicting *E* from mineralogical and petrophysical variables. The findings of this study will provide the Kansas Department of Transportation (KDOT) with a comprehensive understanding of local limestone aggregates and thus contribute to improved material selection and aggregate quality evaluation.

Chapter 2 - Materials and Methods

In this study, uniaxial compression tests were performed on all core samples (1-inch and 2-inch) in the Department of Civil Engineering at Kansas State University. The value of *E* was calculated from the stress-strain experiments. All mineralogical analyses of 1-inch cores and aggregate samples were conducted in the Department of Geology at Kansas State University. For 2-inch cores, all mineralogical analysis was performed at the Illinois State Geological Survey X-ray Diffraction (XRD) and X-ray Fluorescence (XRF) Laboratory. Mineralogical composition was determined by bulk XRD analysis and clay fraction XRD analyses (<2 μm), each requiring distinct sample preparation and analytical procedures. The following sections describe the sampling process, mechanical testing procedures, saturation process, and mineralogical techniques.

2.1 Sampling

The Kansas Department of Transportation (KDOT) selected extraction sites and collected core samples from three quarries, which were then delivered to Kansas State University (K-State) for this study. KDOT cored the material into 1-inch diameter before sending them to the University of Kansas (KU), where they were cut into 1-inch and 2-inch-long core plugs (Figures 1 and 2). These core plugs were designated for both *E* testing under wet and dry conditions and mineralogical analysis (Table 1).

A total of 57 core plugs were produced across the three quarries, comprising of 29 1-inch plugs (Figure 2.1) and 28 2-inch plugs (Figure 2.2). Quarry 1 yielded three cores, Quarry 2 two cores, and Quarry 3 two cores. Core plugs were cut from these extracted cores, yielding 14 1-inch and 10 2-inch plugs from Quarry 1, 4 1-inch and 6 2-inch plugs from Quarry 2, and 12 1-inch and 12 2- inch cores from Quarry 3. Within each core, core plugs were categorized alphabetically by depth, with Core Section A corresponding to the interval closest to the surface. After core plugs were extracted, the remaining core segments, or core shells, were returned to K-State and crushed into a total of 39 ¾ -inch aggregates. These aggregates, which each correspond to a core section, were used exclusively for mineralogical analysis (Figure 2.3). To ensure that the crushed material was representative, aggregates were selected from the most lithologically uniform portions of the core shells. Each sample was assigned an identifying sample number. For each sample number, there is one aggregate. Depending on availability of cores, the same interval may also have a 1-inch core plug, a 2-inch core plug, or both. Sample used for dry and wet test conditions do not necessarily correspond to 1-inch and 2-inch pairs that were extracted from the same core or core section, as reported in Table 1.

Table 1 Summary of 1-inch and 2-inch core plug and aggregate samples by number, location, and testing condition.

Sample No.	Quarry	Core	Core Section	Depth (ft)	Aggregates	1-inch Core	2-inch Core
1	1	1	A	5.1 - 5.6	Dry	Dry	Dry
2	1	1	B	6.7 - 7.1	Dry	Wet	-
3	1	1	C	7.1 - 8.6	Dry	Dry	-
4	1	1	C	7.1 - 8.6	Dry	Wet	-
5	1	1	D	10.1 - 11.1	Dry	Wet	Dry
7	1	1	E	11.1 - 12.1	Dry	Dry	Dry
9	1	1	E	11.1 - 12.1	Dry	Wet	Dry
10	1	2	A	3.1 - 4.5	Dry	-	Dry
11	1	2	A	3.1 - 4.5	Dry	Dry	Wet
12	1	3	A	1.8 - 2.7	Dry	Dry	-
14	1	3	B	5.9 - 6.9	Dry	-	Dry
15	1	3	B	5.9 - 6.9	Dry	Dry	-
16	1	3	C	6.9 - 7.5	Dry	-	Wet
17	1	3	D	10.6 - 12.6	Dry	Wet	Wet
19	1	3	D	10.6 - 12.6	Dry	Dry	-
20	1	3	D	10.6 - 12.6	Dry	-	Wet
23	1	3	F	18.3 - 18.7	Dry	Wet	-
24	2	1	A	2.7 - 3.2	Dry	-	Wet

25	2	1	A	2.7 - 3.2	Dry	Dry	-
26	2	1	B	3.5 - 4.15	Dry	-	Wet
27	2	1	B	3.5 - 4.15	Dry	Wet	-
28	2	1	C	5 - 5.3	Dry	-	Dry
29	2	2	A	1.8 - 2.2	Dry	Dry	-
30	2	2	B	3.3 - 3.8	Dry	-	Dry
32	2	2	C	3.8 - 4.3	Dry	-	Dry
33	2	2	C	3.8 - 4.3	Dry	Wet	-
34	2	2	D	5.3 - 5.75	Dry	-	Dry
35	3	1	A	3.9 - 4.6	Dry	Dry	Dry
36	3	1	B	8.9 - 9.4	Dry	Dry	Wet
37	3	1	C	13.9 - 15	Dry	Dry	Dry
38	3	1	D	19.7 - 20.2	Dry	Dry	Wet
39	3	1	E	27.3 - 27.8	Dry	Wet	Dry
40	3	1	F	29.7 - 30.2	Dry	Wet	Wet
41	3	2	A	4.4 - 4.9	Dry	Wet	Wet
42	3	2	B	9.1 - 9.6	Dry	Dry	Wet
43	3	2	C	13.4 - 13.9	Dry	Wet	Wet
44	3	2	D	21.5 - 22.1	Dry	Dry	Wet
45	3	2	E	26.4 - 26.9	Dry	Wet	Wet
46	3	2	F	30.3 - 30.8	Dry	Wet	Wet

Figure 2.11-inch core samples used for uniaxial compression tests and mineralogical analysis.

Figure 2.2 2-inch core samples used for uniaxial compression tests and mineralogical analysis.

Figure 2.3 Crushed ¾-inch limestone aggregates used for mineralogical analysis.

2.2 Young's Modulus

E was determined from uniaxial compression tests performed on the 57 core samples described in Section 2.1. Testing procedures followed the guidelines outlined in the American Society for Testing and Materials (ASTM) Method D-7012. All tests were conducted using a Shimadzu AG-IC loading device with a constant stress rate of 0.75 MPa/s. Strain measurements were recorded using 350-ohm surface-mounted electrical resistance strain gages. Bond 200 adhesive was used to adhere strain gages to dry specimens, while M-Bond AE-10 was used to secure strain gages for saturated test conditions. Strain data was collected using a P-3500 strain indicator and logged by a Keithley 2700 multimeter and data acquisition system. The experimental setup, including the Shimadzu AG-IC loading device, P3500 strain indicator, and Keithley 2700 data acquisition system, is shown in Figure 2.4. Two strain gages were mounted on opposite sides on the lateral surface of each core sample. This helped to account for potential surface irregularities, unleveled surfaces, and overall variability in strain measurements. For each specimen, the value of *E* was calculated from the gage that showed the most consistent and representative linear response.

In accordance with ASTM D7012-23, *E* was calculated from the slope of the straight-line portion of the stress-strain curve. The slope was calculated by dividing the change in stress by the change in strain, as expressed by the following equation:

$$E = \frac{s}{e} \quad (1)$$

where E is Young's modulus (GPa), s is uniaxial stress, and e is strain.

Figure 2.4 Experimental setup for uniaxial compression tests, including the Shimadzu AGIC loading device, P3500 strain indicator, and Keithley 2700 data acquisition system

2.3 Volumetric Water Content

A total of 29 core samples were allocated to wet test conditions, with the distribution of wet and dry samples provided in Table 1. Core plugs designated for wet testing conditions underwent a different strain gage attachment procedure. Prior to water exposure, strain gages were attached and sealed with M-Bond AE-10, a 100% solids epoxy system, to ensure secure attachment during water exposure.

Samples were first placed in a glass vacuum desiccator and submerged in deionized water, where they were left to soak for 24 hours to help promote saturation (Figure 2.5). After, a vacuum of approximately 30 in-Hg was applied using a connected vacuum pump to release entrapped air in the core plugs. The vacuum was maintained until no release of air was observed. The samples were weighed before and after vacuum saturation to quantify water intake. Porosity data was unavailable and full saturation conditions are not confirmed. The θ was used in this study as a proxy for porosity, given that porosity was unavailable. θ was calculated using the direct mass-based method:

$$\theta = \frac{V_W}{V_T} \tag{2}$$

where V_W is the volume of water and V_T is the total volume of the sample. θ is represented as a percent throughout this study.

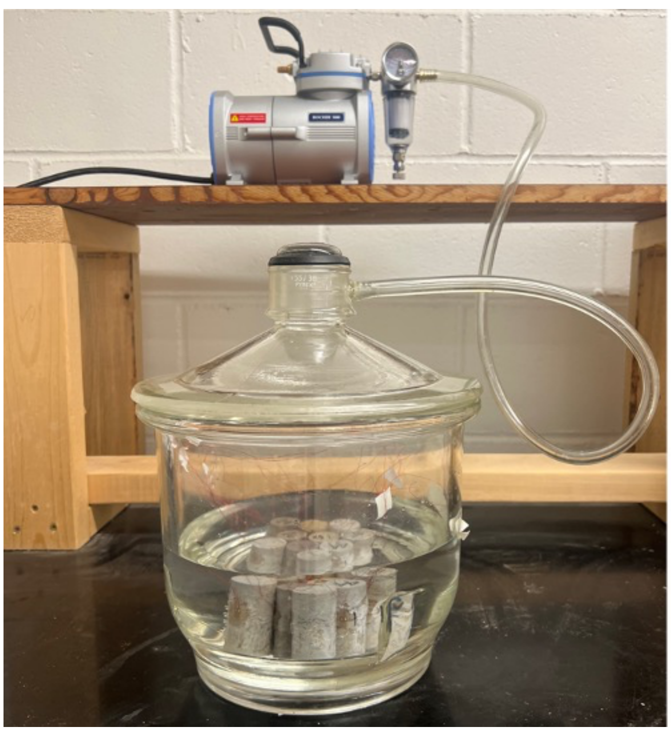

Figure 2.5 Vacuum saturation setup with glass desiccator, deionized water, connected vacuum pump, showing submerged core samples.

2.4 Bulk Mineralogy

Bulk powder XRD analysis was performed on all samples using the powder X-ray diffraction (XRD) method. Analyses were conducted using a PANalytical Empyrean X-ray diffractometer to quantify the percentages of calcite, dolomite, quartz, and other minerals in each sample, following the procedures outlined by Adatte et al. (1996). To prepare each sample for XRD, any residual epoxy or adhesive from the strain gage was removed via sanding. Samples that had undergone vacuum saturation were air-dried and then oven-dried at 50 °C to remove residual moisture. The rock samples were manually ground using a mortar and pestle into a fine powder, and the resulting powder was mounted onto zero-background holders. To obtain a more representative bulk composition, each core was first coarsely crushed to incorporate material from the entire sample.

The XRD was operated at 45 kV and 80 mA and equipped with a Cu tube. Samples were scanned from 5° to 80° 2θ with a step size of 0.03° and a goniometer speed of 0.5°/min. Phase quantification was performed using the Rietveld refinement method in Profex software (Doebelin & Kleeberg, 2015).

2.5 Clay Mineralogy

The clay fraction analysis was conducted to identify and semi-quantify clay minerals present in the <2 μm size fraction, as defined by ASTM standards. To prepare samples, residual epoxy or adhesive from mechanical tests was removed from all core surfaces with a sander. Wet samples were first air-dried, and then oven dried at 50° C to remove residual water. Samples were treated with hydrochloric acid (HCL) to remove non-clay phases, followed by centrifugation to isolate the clay-sized fraction, and lastly, mounted on glass slides (Figure 2.6). All samples underwent ethylene glycol solvation treatment at 50° C for 24 hours to identify the presence of swelling clays based on their expansion behavior. The XRD analysis was performed on oriented mounts in both air-dried and glycolated samples using a PANalytical Empyrean diffractometer, with a scan range of 3.5°-50° 2θ and a step size of 0.03°. Diffractograms were processed and analyzed using the MacDiff software (version 4.2.5), with interpretation aided by Moore and Reynolds (1997). Clay minerals were identified based on their characteristic basal reflections observed in the diffractograms of the air-dried and ethylene glycol-treated samples. Illite was identified by its (001) and (002) reflections near 10 Å and 5 Å, chlorite by its (001), (003), and (004) reflections near 14 Å, 7Å, and 3.54 Å, and kaolinite by its (001) and (002) reflections near 7.1 Å and 3.57 Å. Smectite was identified in ethylene glycol-solvated preparations by its (001) reflection at 17 Å, reflective of its swelling behavior. Semi-quantitative clay mineral proportions were based on peak intensity ratios derived from the (004) reflection of chlorite at 3.54 Å, the (001) reflection of illite at 10 Å, the (002) reflection of kaolinite at 3.57Å, and the (001) reflection of smectite at 17 Å. These percentages are semiquantitative and represent the relative proportions of chlorite, illite, kaolinite, and smectite within the clay fraction, rather than absolute or weight percentage in the sample.

Figure 2.6 Prepared glass slides for clay fraction (<2μm) X-ray diffraction

Chapter 3 - Results and Discussion

This chapter presents the results of the uniaxial compression tests conducted on 57 limestone core samples, along with mineralogical analyses conducted on 57 core and 39 aggregate samples. *E* was examined in terms of saturation condition, core size, and mineralogical composition. The complete dataset, including individual measurements and sample information, is provided in Appendix A.

Across all 57 core samples tested under uniaxial compression, *E* ranged from 3.9 to 53.4 GPa, with a mean of 27.1 GPa. Summary statistics for *E* are provided in Table 2. The mean *E* for the 28 dry cores was 29.9 GPa, compared to 24.4 GPa for the 29 wet cores, reflecting a mean reduction of approximately 18.4% GPa. When comparing by core size, 1-inch cores exhibited the mean *E* value of 28.9 GPa, while 2-inch cores averaged 25.2 GPa.

Table 2 Summary of Young's Modulus *E* measured under both dry and wet conditions, with corresponding volumetric water content θ.

Core	Condition	E_{mean} (GPa)	θ_{mean} (%)
1-inch	Dry	28.9 ± 11.8	-
1-inch	Wet	27.3 ± 10.9	8.4 ± 4.4
2-inch	Dry	29.3 ± 9.2	-
2-inch	Wet	21.6 ± 12.7	9.1 ± 5
All Cores	Dry	29.9 ± 11.6	-
All Cores	Wet	24.4 ± 12.0	8.8 ± 4.6
All Cores	Dry +Wet	27.1 ± 11.8	-

3.1 Young's Modulus and Mineralogy

3.1.1 Young's Modulus and Bulk Mineralogy

Relationships between *E* and mineralogy were assessed across the full dataset, including both dry and wet core samples. Summary statistics for mineral contents are provided in Table 3, and a representative diffractogram showing the primary peaks for calcite, dolomite, and quartz is shown in Figure 3.1. Corresponding scatter plots of *E* against bulk mineralogy are shown in Figure 3.2. As demonstrated, calcite content ranged from 4.0 to 98.3%, with a mean of 88.2%. Although the highest *E* values (> 40 GPa) were all observed in core samples containing an average of 90% calcite, many samples with lower *E* values also contained high levels of calcite. This suggests that although calcite is necessary for baseline stiffness in limestone, it does not control the variability of *E* across the dataset. The lack of a distinct trend between calcite and *E* may also reflect the narrow distribution range of calcite. Dolomite ranged from 0.0 to 93.3%, with an average of 8.3%. 81% of all core samples contained less than 10% dolomite. One sample with an outlier of 93.8% dolomite corresponded to the lowest *E* value of 3.8 GPa. Yale (1994) suggested that a threshold of 30% dolomite might be required to increase the *E* in limestones. Only two samples exceeded 30%, both corresponding to relatively low moduli (>20 GPa). One contained 93.3% dolomite and had the lowest *E* in the dataset at 3.9 GPa. The other contained 31.5% dolomite and had an *E* value of 19.9 GPa. Samples with varying dolomite concentrations showed both high and low *E* values, suggesting that dolomite is unlikely to control *E*. Quartz content was consistently low, ranging from 0.08 to 4.5%, with an average of 1.4% Across the entire dataset, quartz did not explain variability in *E*, likely due to the low quartz content observed.

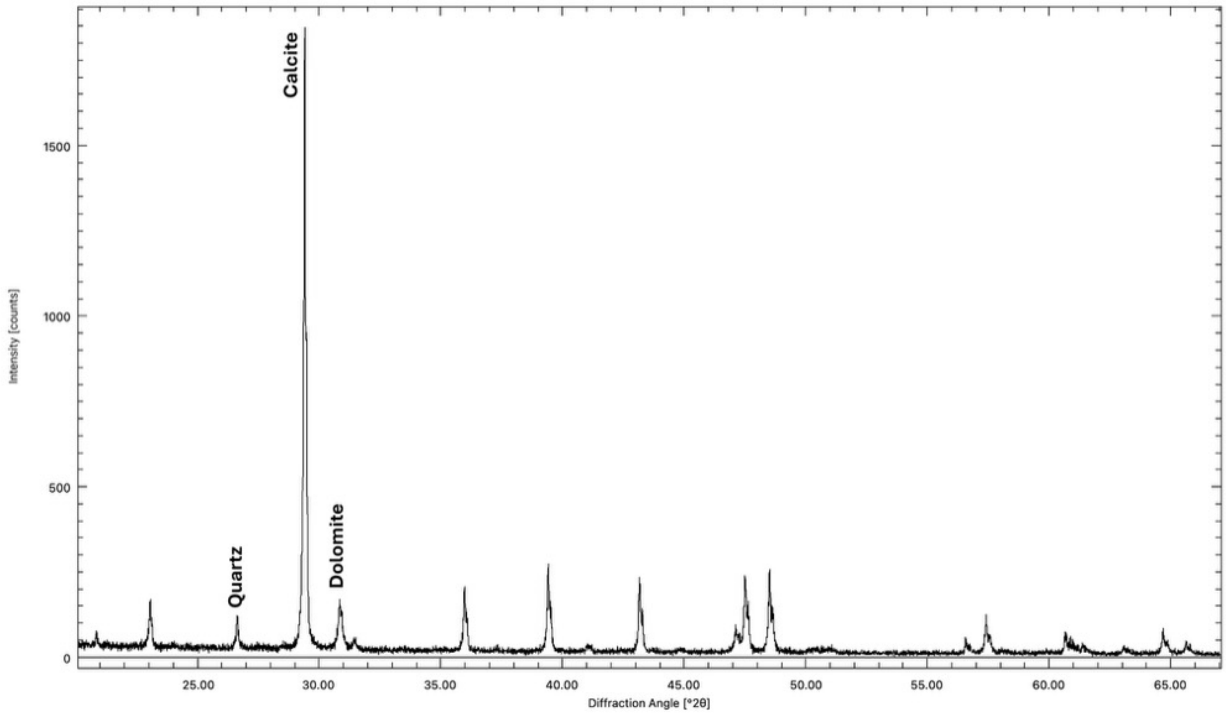

Figure 3.1 X-ray diffractogram of bulk powder from a representative 1-inch core sample, with labeled diagnostic peaks for calcite, dolomite, and quartz.

Table 3 Average and one standard deviation of bulk mineral content reported for calcite, dolomite, and quartz (%).

Sample	Condition	$\text{Calcite}_{\text{mean}}$ (%)	$\text{Dolomite}_{\text{mean}}$ (%)	$\text{Quartz}_{\text{mean}}$ (%)
Aggregates	Dry	89.7 ± 15.8	7.8 ± 16.2	2.3 ± 0.9
1-inch Cores	Dry	89.7 ± 23.8	8.7 ± 23.5	1.7 ± 0.8
	Wet	88.2 ± 10.5	9.5 ± 10.8	2.3 ± 1.3
	Dry +Wet	89 ± 18.3	9 ± 18.2	2 ± 1.1
2-inch Cores	Dry	89.8 ± 3.6	5.5 ± 2.6	1.2 ± 1
	Wet	85.2 ± 7.1	9.3 ± 6.2	0.7 ± 0.3
	Dry +Wet	87.4 ± 6.1	7.5 ± 5.2	0.9 ± 0.7
All Cores	Dry +Wet	88.2 ± 13.7	8.3 ± 13.4	1.4 ± 1.1

Across the entire dataset, the bulk mineral content did not sufficiently explain the variability observed in *E*. While high calcite is necessary for baseline stiffness and strength in limestones due to its role as the primary constituent of limestone, its narrow range within this dataset limits its control. Prior research on high carbonate limestones (>97.6% calcite and dolomite) has shown that samples with higher dolomite content, rather than calcite, exhibit higher E. This suggests that dolomite may contribute more to stiffness than calcite (Yan et al., 2022). As a diagenetic product, dolomite is more likely evenly distributed, allowing even small concentrations to stiffen the rock framework (Yale et al., 1994). Yale (1994) also noted that the stiffening effect of dolomite may be offset if quartz or clay content exceed 15%. However, in this study, quartz content was low ($\leq$ 4.5%) and is unlikely to suppress dolomite-related strengthening. At the microscale, carbonate grains, such as calcite and dolomite, exhibit higher intrinsic E than quartz, as demonstrated by nanoindentation tests conducted by Chen et al. (2023). In carbonate rocks, increased quartz concentrations can introduce weak grain boundaries, which can lead to E reductions. In contrast, in rocks where quartz is more abundant, increased quartz content has been associated with higher E values. For instance, Wang et al. (2022) found a strong positive correlation with quartz content (R^2 = 0.88) in Lower Cambrian shales and a negative correlation with clay mineral content (R^2 = 0.73). They found that samples with similar quartz content exhibited different modulus values depending on porosity, with lower porosity corresponding to higher E. This suggests that other factors, such as porosity, may exert an influence on E even when mineralogy remains constant. A similar trend was observed in sandstones analyzed by Sujatono and Wijaya (2022), who found that 1% increase in quartz content was associated with a 5% increase in axial E and a 2.4% increase in diametral E. They attributed the increase in stiffness to frictional pressure acting on heterogeneous quartz grains, which causes finer grains to deform and fill in voids under pressure.

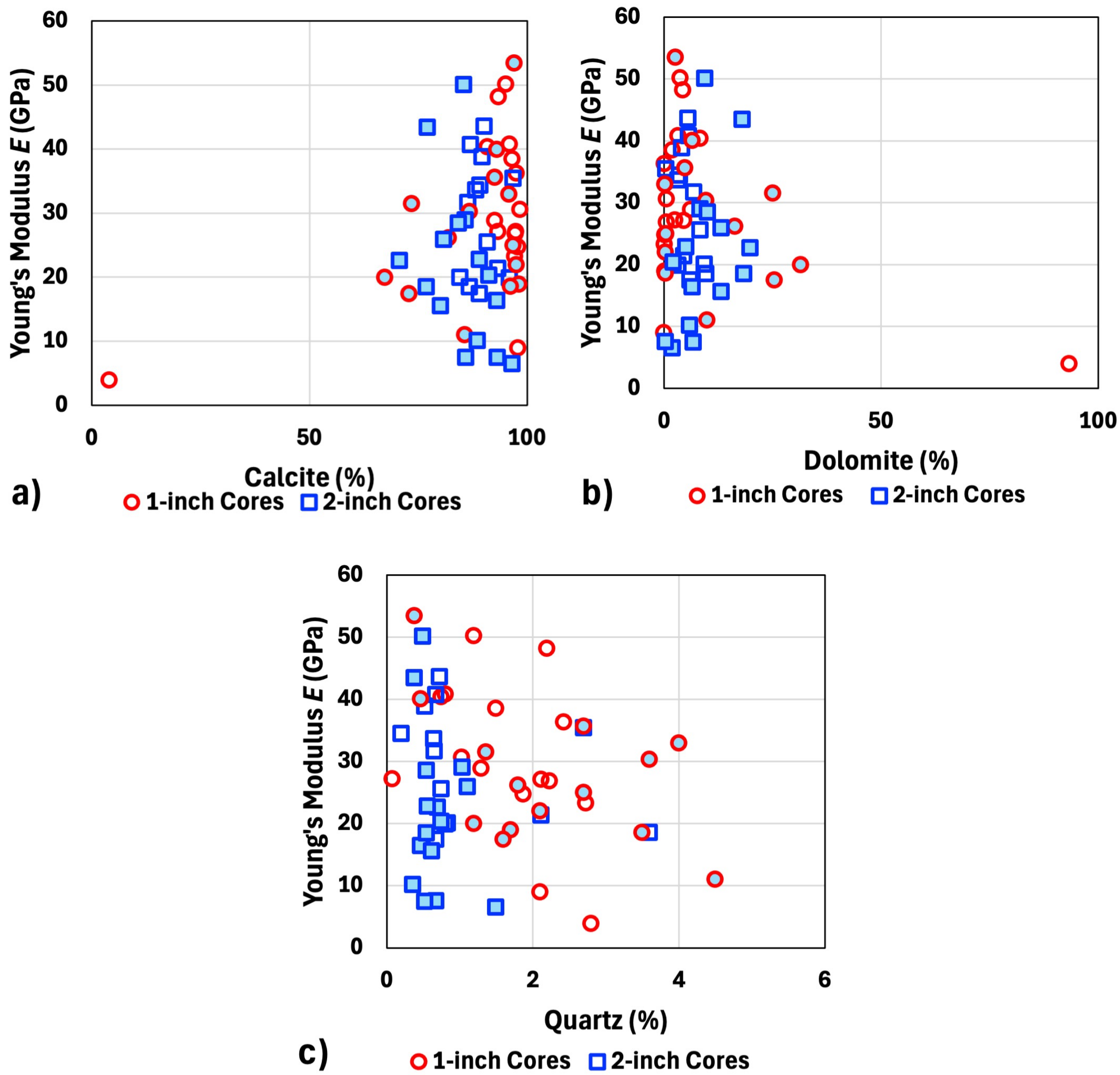

Figure 3.2 Young's modulus *E* plotted against bulk mineralogy for (a) calcite, (b) dolomite, and (c) quartz content (%) in 1-inch and 2-inch cores. Blue-filled markers indicate wet samples, while dry samples are represented by unfilled markers.

3.1.2 Young's Modulus and Clay Mineralogy

Relative proportions of chlorite, illite, kaolinite, and smectite are summarized in Table 4, with clay mineral distributions illustrated in Figure 9. Illite was the most abundant clay mineral, ranging from 26 to 94.7%, with a mean of 69.4%. Chlorite content ranged from 0% to 34%, with an average of 10.9%. Kaolinite ranged from 0.0 to 67.6%, with a mean of 16.8%. Smectite was present in low proportions, ranging from 0.0 to 18.3%, with a mean of 2.8%. Only three samples contained more than 10% smectite, and 58% of the samples did not contain any smectite. The distributions show that the clay fraction is dominated primarily by illite, with moderate amounts of chlorite and kaolinite, and only minor amounts of smectite. When plotted against E (Figure 3.3), no clay mineral showed a consistent or clear trend. However, these values only represent the relative proportions of clays within the clay fraction, rather than the weight percentage in the rock. The absence of a consistent trend suggests that, within this dataset, differences in clay composition alone do not explain the observed variability in E.

The clay fraction in this dataset was dominated by non-swelling minerals, including illite, chlorite, and kaolinite. Smectite only occurred in trace amounts, with over half of the samples containing no smectite. The minor presence of smectite suggests that the clay-related weakening observed in other studies may not be a contributing factor in this dataset. This contrasts with findings from previous studies, where increasing clay content, especially swelling clays, resulted in E reductions. For instance, Chen et al. (2022) examined a smectite-rich mudstone containing 90% smectite within a total clay content of 50.3% and reported a 95.9% reduction in E as the water content increased from 0 to 10%. They attributed this significant weakening to smectite hydration and swelling, which increases water film thickness, disrupts interparticle bonds, and promotes microcracking via matrix dissolution and shear dislocation. However, in the present study, these mechanisms are unlikely to dominate given the minor concentrations of smectite. Although clay content varied across the dataset, no relationship was observed between the relative abundance of any clay mineral and E. This may reflect the use of relative proportions of clay content, rather than absolute measurements or suggest E reductions are not primarily driven by smectite-related weakening. Mineralogy is further explored in section 3.2, where it is analyzed with E and θ.

Table 4 Average and one standard deviation of clay content (< 2 μm) reported for illite, chlorite, kaolinite, and smectite (%)

Sample	Condition	$\textbf{Illite}_{\textbf{mean}}$ (%)	$\textbf{Chlorite}_{\textbf{mean}}$ (%)	$\textbf{Kaolinite}_{\textbf{mean}}$ (%)	$\textbf{Smectite}_{\textbf{mean}}$ (%)
Aggregates	Dry	65 ± 19.1	15.4 ± 6	18 ± 22.5	1.6 ±2.5
1-inch	Dry	61.1 ± 24	13.4 ± 3.6	24.3 ± 27.4	1.2 ± 2.1
	Wet	60.5 ± 22.8	14.9 ± 4.8	23.1 ± 26	1.6 ± 3.2
	Dry +Wet	60.8 ± 23	14.1 ± 4.2	23.7 ± 26.3	1.4 ± 2.6
2-inch	Dry	82.4 ± 11.2	5.5 ± 3.3	7.6 ± 7.5	4.5 ± 5
	Wet	74.8 ± 12.7	9.6 ± 7.6	11.5 ± 10	4 ± 5.2
	Dry +Wet	78.3 ± 12.4	7.7 ± 6.2	9.7 ± 9	4.3 ± 5
All Cores	Dry +Wet	69.4 ± 20.4	10.9 ± 6.2	16.8 ± 20.8	2.8 ± 4.2

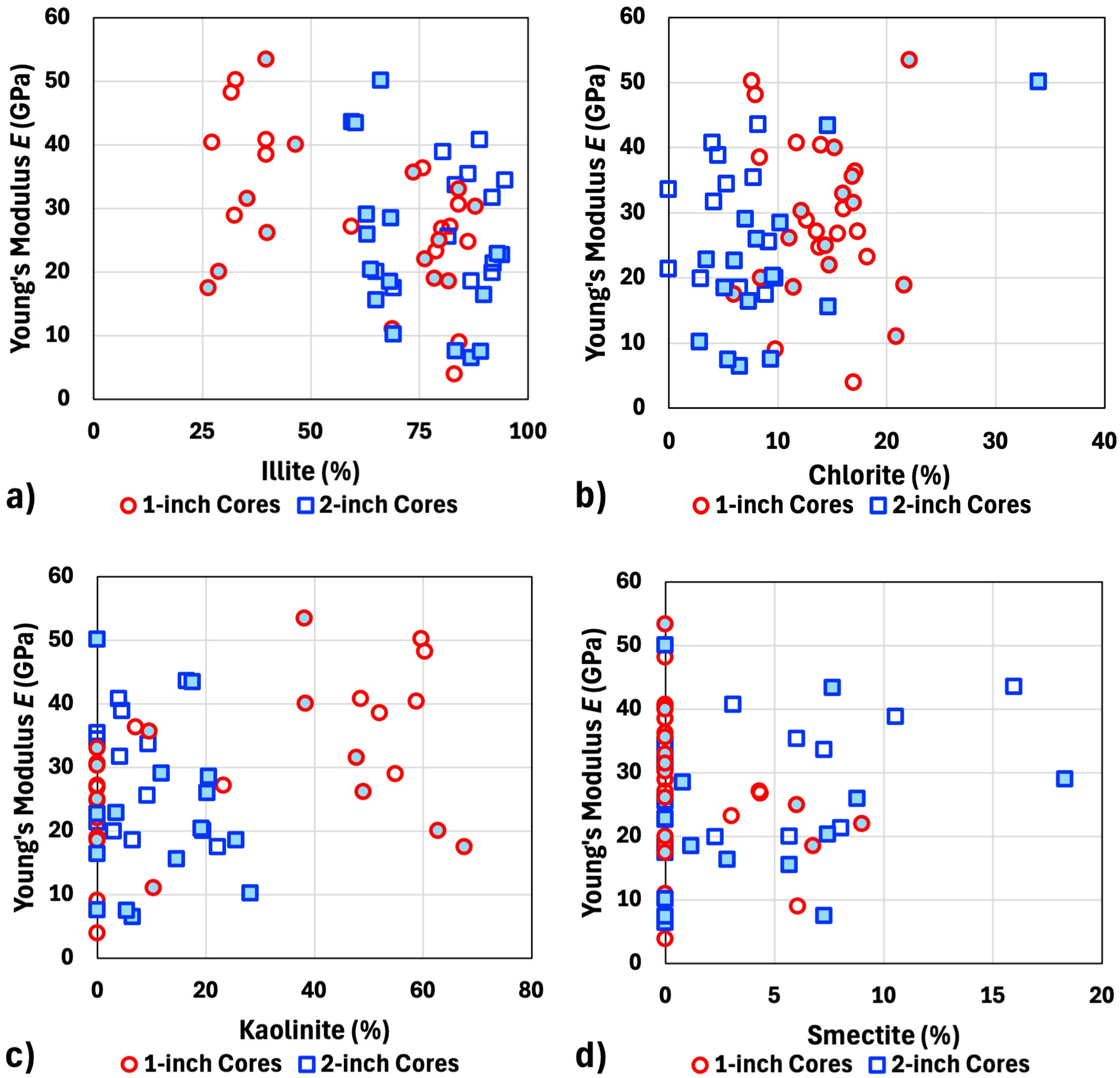

Figure 3.3 Young's Modulus *E* as a function of the clay fraction (<2 μm) for (a) chlorite, (b) illite, (c) kaolinite, and (d) smectite content (%). 1-inch cores are shown as red-outlined circles, and 2-inch cores as blue-outlined squares. Blue-filled symbols indicate wet samples, and dry samples are indicated by unfilled markers.

3.2 Young's Modulus and Volumetric Water Content

3.2.1 Young's Modulus under Wet and Dry Conditions

The frequency distribution of *E* for all limestone core samples is shown in Figure 3.4. As summarized in Table 2, our results show that *E* decreased from 29.9 GPa in dry core samples to

24.4 GPa in wet samples, representing an average *E* reduction of 18.4%. However, this average does not entirely capture the variability observed among wet and dry core samples. A comparison of dry and wet *E* values across all cores showed considerable scatter and revealed no relationship between wet and dry *E* (Figure 11). Student t-tests, assuming unequal variance, were conducted to test whether the difference between wet and dry *E* was statistically significant. The null hypothesis states that there is no statistically significant difference in *E* between the two groups tested. A 95% confidence interval was used. A p-value less than 0.05 was considered statistically significant and supports rejecting the null hypothesis. No statistically significant difference was found between *E* measured in dry and wet core samples, as confirmed by p-value = 0.24.

Overall, these results indicate that the amount of *E* reduction due to saturation is not uniform, nor is it determined by the dry *E* value. In our dataset, dry *E* is not a predictor of wet *E*. Our results contrast with previous studies, such as Vásárhely (2005), who found a strong linear correlation between wet and dry *E*, suggesting a proportional reduction in *E* (R^2 = 0.87). Similarly, Daraei and Zare (2018) found a strong power-law relationship between wet and dry *E* (R^2 = .74). However, their study also emphasized that even among carbonate limestones, the reduction in *E* varied significantly, with two limestones showing 43% and 69% reductions, respectively. This variability in *E* was attributed to differences in mineralogy, clay content, porosity, and other petrophysical and geomechanical properties that may influence how water interacts with the rock. Specifically, calcite and quartz-filled cracks were associated with lower reductions, while clay-rich and silty zones were associated with higher reductions. Similar mechanisms may contribute to the heterogeneous *E* reductions observed in our dataset.

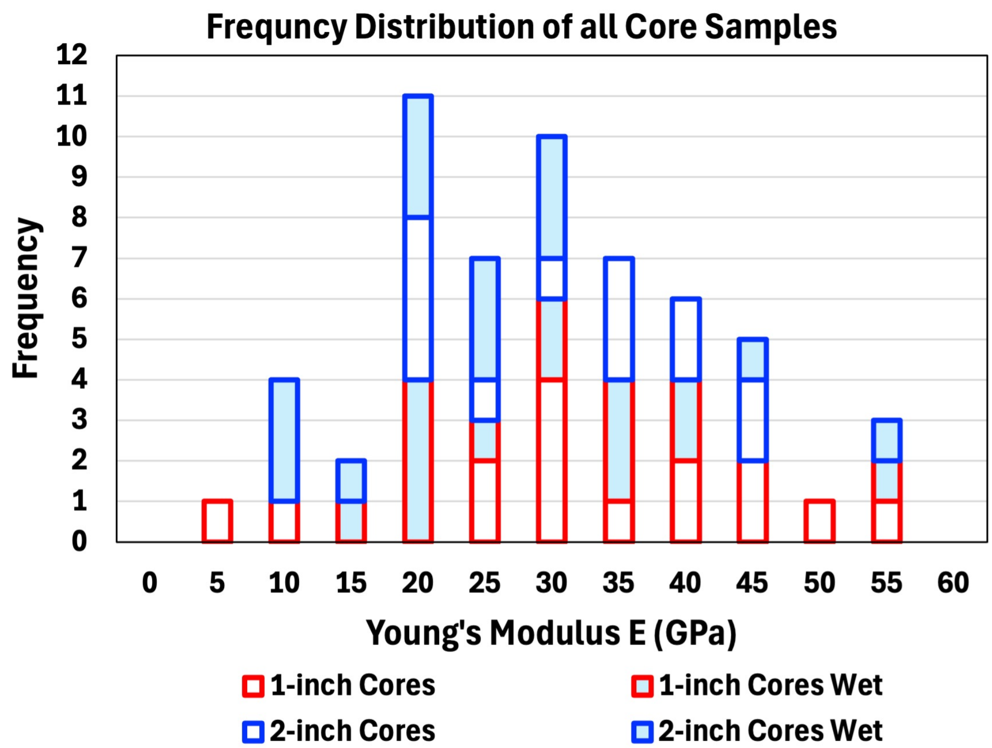

Figure 3.4 Frequency distribution of Young's modulus *E* for all limestone core samples. Red-outlined portions represent 1-inch cores and blue-outlined segments represent 2-inch cores. Blue-filled portions indicate wet samples, while dry samples are unfilled.

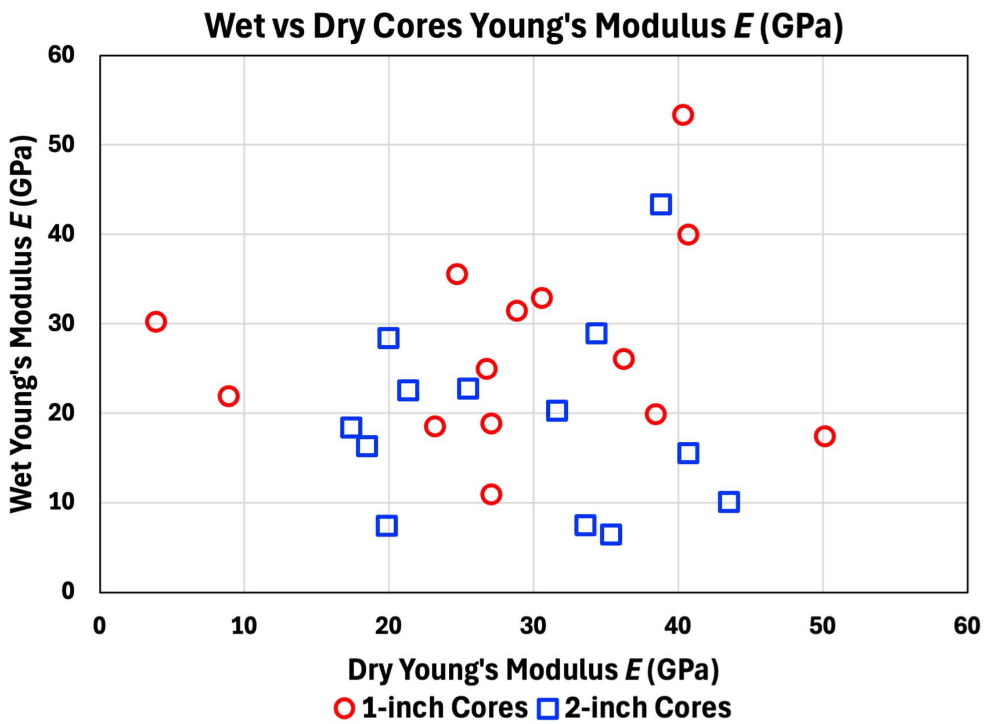

Figure 3.5 Wet vs. dry Young's modulus *E* for 1-inch and 2-inch cores. 1-inch cores are shown as red-outlined circles, and 2-inch cores as blue-outlined squares.

3.2.2 Young's Modulus and Volumetric Water Content

To further explore the influence of θ, *E* was also examined as a function of θ (Figure 3.6). Among the 29 wet limestone cores, θ ranged from 0.96% to 18.7%, with an average of 8.8± 4.6%. Figure 3.6 illustrates the inverse relationship between *E* and θ. 44.8% of wet core samples exceeded mean *E* of 24.4 GPa, while 55.2% fell below it. When comparing θ between these two groups, samples with *E* above the average had a mean θ of 6.1%, whereas samples with below average *E* had a mean θ of 11%. All samples with *E* exceeding 40 GPa, which correspond to a relatively high *E* in our samples, exhibited θ below 5.1%. The lowest modulus (6.46 GPa) corresponded to the highest θ (17.2%), while the highest *E* (53.4 GPa) corresponded to a relatively low θ (3.6%). These results suggest that limestone samples with higher θ tend to exhibit overall greater reductions in *E*.

Comparable findings have been reported in the literature. For instance, Zhang et al. (2021) reported a 30% reduction in *E* for Yunnan limestone with a small increase in gravimetric water content from 0.1% to 0.5%, highlighting limestone's sensitivity to moisture at low saturation. In comparison, Lashkaripour et al. (2018) estimated an average reduction of 20% (3.38 GPa) in the *E* of Asmari Limestone after 48 hours of water immersion. Similarly, an average reduction of 18.6% (5.37 GPa) was estimated from five types of limestone reported by Noel et al. (2024). Such reductions in *E* may result from the saturation-driven weakening mechanisms reported in the literature, including reduced effective grain contact, increased pore pressure buildup, and clay-related processes such as swelling and interparticle slip.

Similar trends have also been documented across various rock types. Roy et al. (2017) found that increasing saturation reduced *E* by 18, 27.1, and 20% in Dholpur, Jabalpur white, and Jabalpur red sandstones, respectively, while Jharia shale experienced a much greater reduction of 75%. In Berea sandstone, which is relatively homogeneous in grain and pore size, Kim et al. (2019) found that *E* was 5% higher for the dry samples than the saturated samples. For shales, Lin and Lai (2013) found that *E* decreased by 6.1% for every 1% increase in water saturation. They attributed this reduction to capillary pressure, where high capillary pressure enhances inter-grain adhesion. As saturation increases, these forces decrease and reduce *E*.

Overall, the results from the present study show that θ generally reduces *E* in Kansas limestone, though the degree of reduction varies across samples. This variability highlights the importance of considering mineralogical composition, which is further examined in the following section.

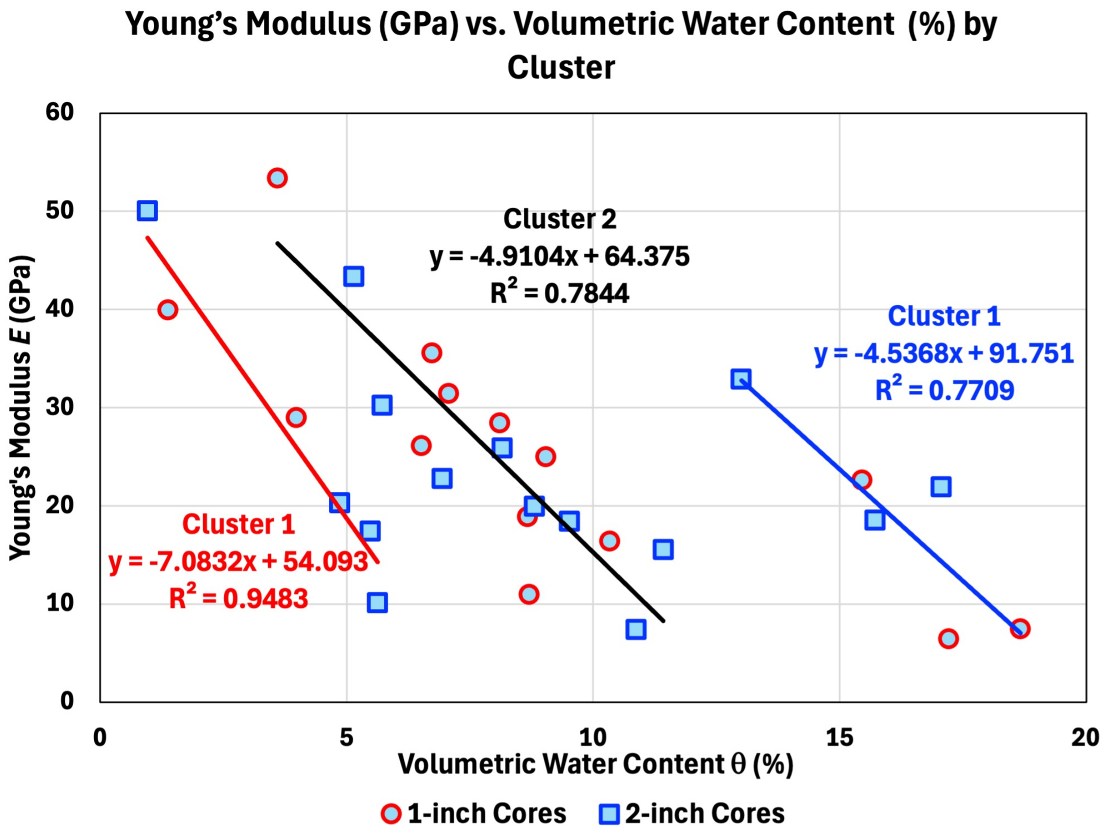

Figure 3.6 Young's Modulus *E* plotted as a function of volumetric water content θ for 1-inch and 2-inch wet core samples. Three distinct clusters (Cluster 1, 2, 3) are plotted with corresponding linear regression equations and R^2 values. Blue-filled markers represent wet samples, and unfilled markers represent dry samples.

3.2.3 Predictive modeling of Young's Modulus

To better interpret the variation in *E* among the wet core samples, a clustering approach was applied. Three clusters (Clusters 1, 2, and 3) were identified and defined based on trends observed between *E* against θ in Figure 3.6. Each cluster was defined by a distinct range of *E* and θ, and separate regression equations were fit to each cluster. The regressions of *E* against θ yielded R^2 values of 0.95, 0.78, and 0.77 for Clusters 1 through 3, respectively, with the corresponding equations provided in Figure 3.6. Cluster 1 (n = 6) had the lowest average θ (3.71%) and the highest average modulus (27.8 GPa). In contrast, Cluster 3 (n = 6) had the highest average θ (16.2%) and the lowest average *E* (18.3 GPa). Cluster 2 (n = 17) was intermediate in θ (8%) but showed similar *E* values to Cluster 1 (25.3 GPa). When *E* was regressed against θ within each cluster, strong negative linear trends ($R^2 \geq 0.77$) were observed. The steepest slope was found in Cluster 3, reflecting a greater reduction in *E* with increasing θ. These patterns indicate that θ is the dominant factor controlling the *E* reduction, even across the relatively narrow saturation ranges within each cluster. θ ranges from approximately 1-6% in Cluster 1, 3.6-11.4% in Cluster 2, and 13-19% in Cluster 3, showing a progressive increase of θ.

While θ appears to be the primary driver of cluster separation, other factors, such as mineralogy, may also contribute to the observed differences. This observation aligns with Daraei and Zare (2018), who found that saturation alone did not account for *E* reductions. Instead, they observed that differing degrees of saturation led to distinct decline patterns, indicating that reductions in mechanical properties also depend on internal factors, such as porosity, density, and fabric, and external factors, including strain rate, surface tension, and suction pressure.

Across the three clusters, mineralogical trends were also explored. lllite increased from Cluster 1 to Cluster 3, reflecting the decrease in *E* with a rise in θ. Kaolinite showed the opposite pattern, decreasing from 27.5% in Cluster 1 to 1.1% in Cluster 3. Chlorite remained relatively stable between Clusters 1 (12.4%) and Cluster 2 (12.6%), then decreased slightly in Cluster 3 (10.7%). Cluster 2 had higher mean illite (66.3% vs. 55.7%) and lower kaolinite (19.12% vs. 27.5%) than Cluster 1. These clay mineral trends reflect a transition from low θ and high *E* in Cluster 1 to high θ and reduced *E* toward Cluster 3.

Although illite is a non-swelling clay, it has been linked to water-related weakening. Supandi et al. (2019) found a strong positive correlation between water content and illite (R = 0.83) in claystones but a weak correlation with kaolinite (R = 0.25), suggesting a stronger influence from illite. They observed that a 1% increase in illite content resulted in a 4% increase in water content, despite representing only 10.8% of the total clay content. The higher proportion of kaolinite in Cluster 1 and its progressive decrease toward Cluster 3 do not necessarily reflect stiffening from kaolinite. This increase in *E* in Cluster 1 may indicate that weaker or swelling clays are simply less abundant in these samples. Chlorite increased slightly in Cluster 3, but its effect on *E* is unclear. However, as a non-expanding clay, its impact is likely minimal.

Dolomite content was slightly higher in Cluster 2 (11.3%) compared to Cluster 1 (9.7%), while calcite remained relatively consistent across all clusters (≥ 85%). Quartz content increased slightly from Cluster 1 (0.8%) to Cluster 3 (2.1%). Notably, Cluster 2 had a higher average θ than Cluster 1 (8% vs. 4%) although both clusters had similar *E* values (25.2 vs. 27.8 GPa). Dolomite is associated with higher *E* due to its stronger Mg-O bonds compared to the Ca-O bonds in calcite (Yan et al., 2022). This may help to explain the relatively high *E* in Cluster 2, despite higher θ. In addition, in quartz-rich rocks, such as sandstone, water molecules can disrupt Si-O bonds through hydrogen bonding, which causes crack propagation and leads to reductions in *E* (Cai et al., 2019). The combination of elevated quartz and illite content may contribute to the lower *E* values observed in Cluster 3, though their influence is difficult to isolate. Nonetheless, these trends are based on numerical and visual summaries of mineral and clay content cross clusters and used to aid in interpretation, explore potential patterns, and analyze relationships among the clusters. However, their overall significance and influence remain uncertain.

To allow for the practical application of the regression models for prediction purposes, three decision trees were created to assign samples to the appropriate clusters based on petrophysical and mineralogical properties (Figures 3.7-3.9). Classification and Regression Tree

(CART) analysis was used to develop decision trees that predict rules for cluster assignment, consistent with the framework established by Breiman et al. (1984). CART is a nonparametric, binary recursive partitioning method used to construct prediction models by segmenting the data (Steinberg, 2009; Loh, 2011). CART models recursively split the data into subsets using decision rules that minimize node impurity, as quantified by the Gini index, and can be represented graphically as decision trees (Breiman et al., 1984; Loh, 2011; Loh, 2014; Steinberg, 2009). In this study, the CART models were implemented using the Python scikit-learn library in Python version 3.13.5. Each tree was trained using the full dataset, with predictor variables including θ, clay mineral percentages (illite, kaolinite, chlorite, and smectite (%), and bulk mineralogy percentages (calcite, dolomite, and quartz (%)). Three different depths were used to cross-validate model performance and provide users different levels of complexity. Trees with larger depths tend to capture minor or conditional thresholds between variables, while trees with low depths tend to capture the most dominant and consistent variables and splits. The three depth settings used were unrestricted (full depth), depth=2, and depth=1.

For each depth, 1,000 CART models were generated using a consistent set of unique random seeds, with the same seeds used across all depths. Generating 1,000 CART models per depth allowed us to capture trends and detect stable and consistent tree structures, which was important given the small dataset (n=29). All models were trained on the full dataset, with the accuracy assessed by 5-fold stratified cross-validation. One final tree was selected at each depth. Final tree selection was based on (1) the frequency of each unique tree structure, (2) the mean cross validation accuracy, and (3) the standard deviation of tree accuracy across all 1,000 models. The final reported decisions trees represent the most consistent and accurate decision trees found at each depth.

The three decision trees all show that θ was the primary classifier for clusters, with consistent thresholds of 12.21 and 5.67%. Results also show that quartz plays a secondary role at lower θ levels of ≤ 5.67%. Cross-validation results show that the full depth tree achieved the highest mean accuracy (80.1% ± 5%), followed by the full depth tree (78.6% ± 5.5 %), and depth=3 tree (76.2% ± 5.7%). These results indicate that θ is the dominant variable controlling cluster separation, while quartz plays a limited secondary role at lower θ. Together, the decision tree and the regression equations form a predictive model to estimates *E* in saturated limestone samples using θ and quartz content.

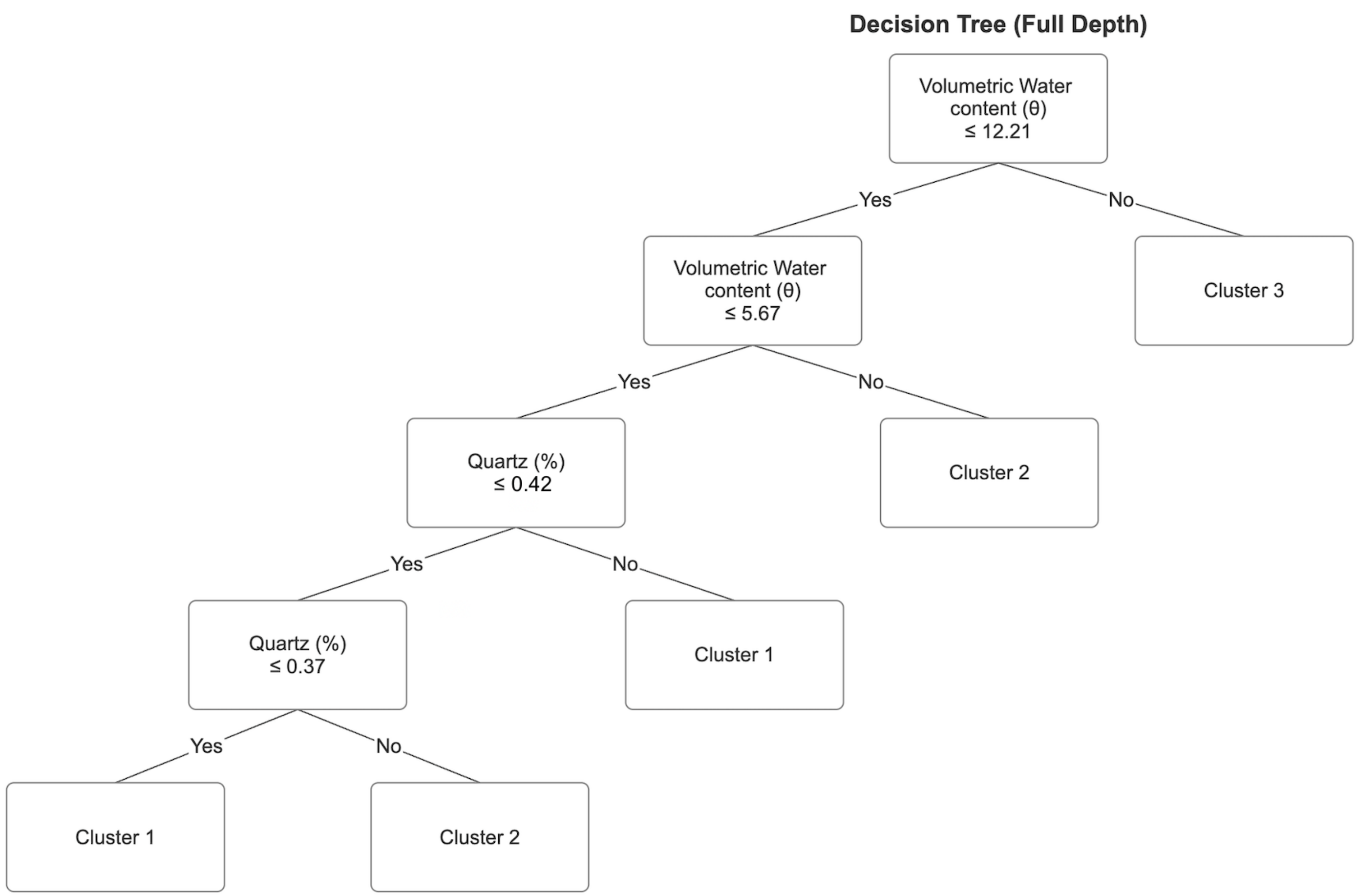

Figure 3.7 Full-depth decision tree constructed using classification and regression tree (CART) analysis to predict cluster assignment. The model was trained on mineralogical data (calcite, dolomite, quartz, illite, chlorite, kaolinite, smectite (%)) and volumetric water content θ.

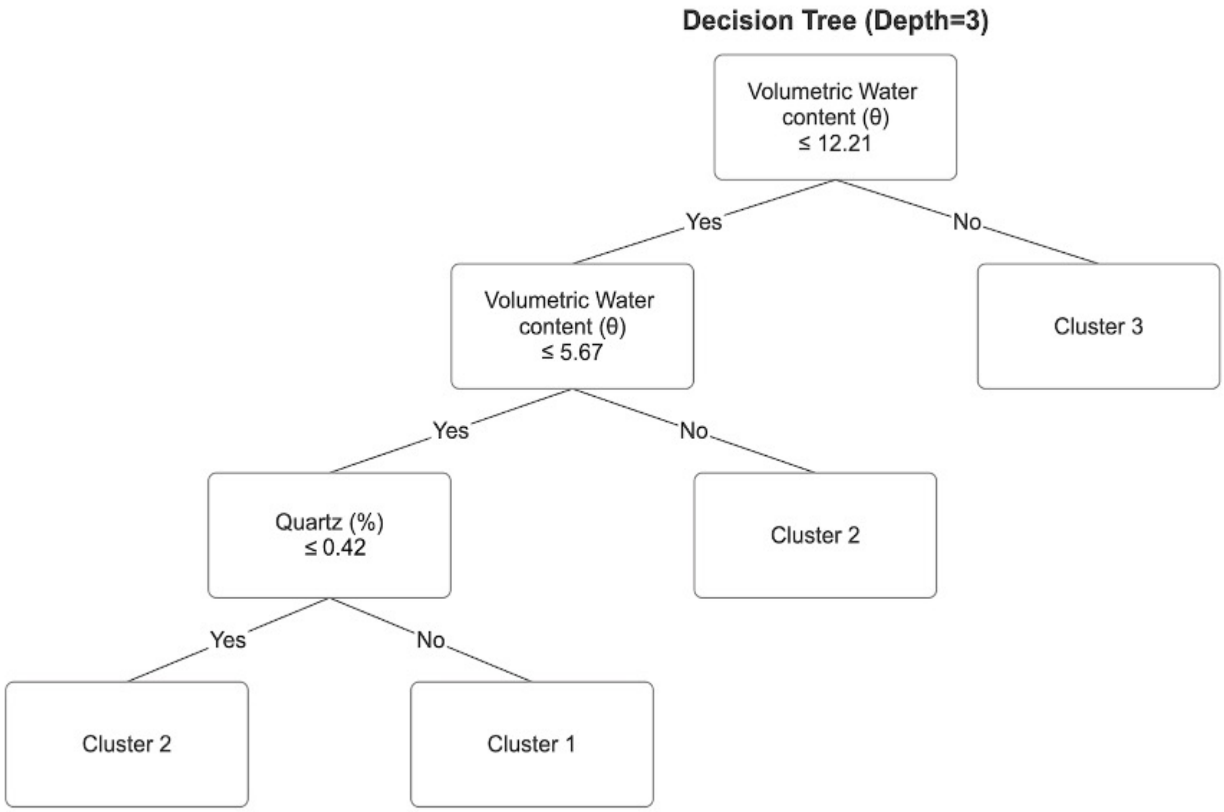

Figure 3.8 Decision tree constructed using classification and regression tree (CART) analysis to predict cluster assignment, with depth= 3. The model was trained on mineralogical data (calcite, dolomite, quartz, illite, chlorite, kaolinite, smectite (%)) and volumetric water content θ.

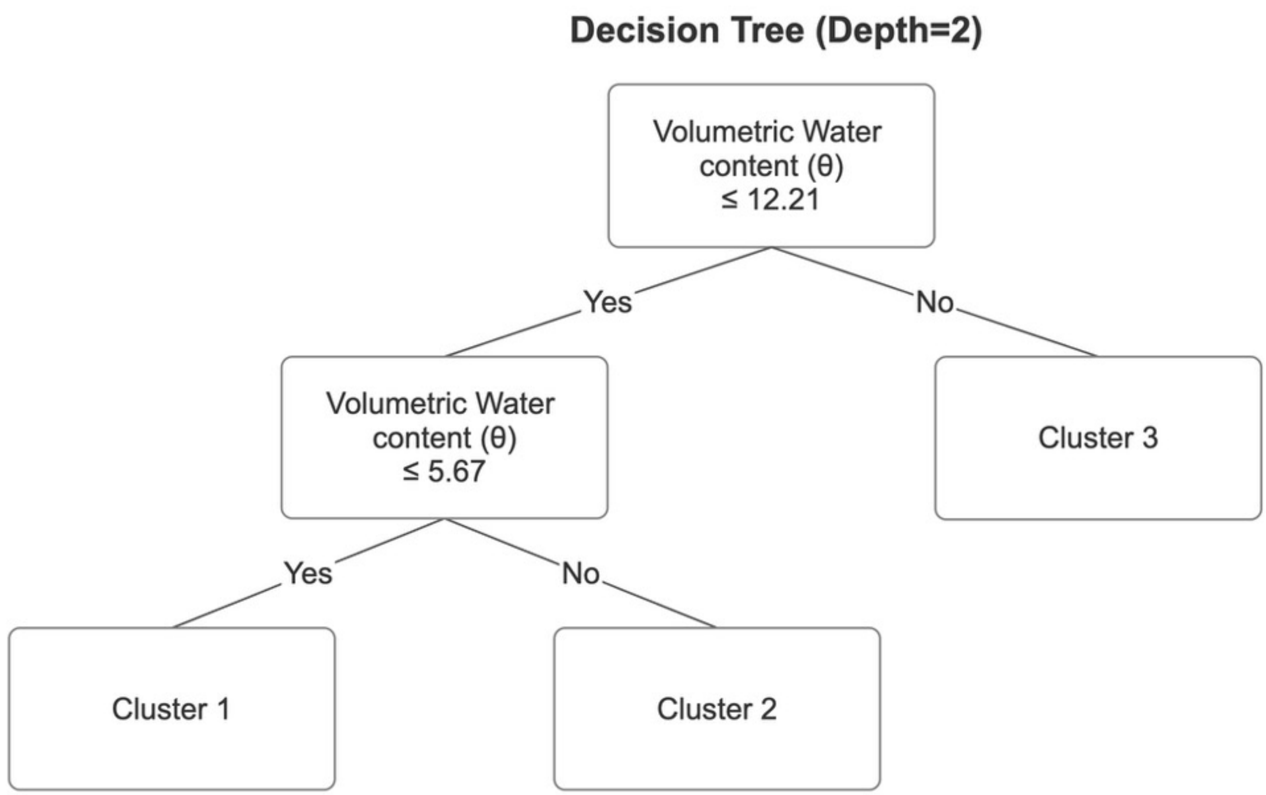

Figure 3.9 Decision tree constructed using classification and regression tree (CART) analysis to predict cluster assignment, with a depth= 2. The model was trained on mineralogical data (calcite, dolomite, quartz, illite, chlorite, kaolinite, smectite (%) and volumetric water content θ.

3.3 Scale Effects

3.3.1 Mineralogical Comparisons Across Scales

Mineralogical comparisons across sample scales were evaluated using scatter plots (Figures 3.10-3.15) and Student t-tests. Bulk mineral trends are shown in Figures 3.10-3.12, and clay mineral trends in Figures 3.13-3.15. Student t-tests, assuming unequal variances, were conducted to evaluate whether mineral content differed significantly between sample sizes. A p-value less than 0.05 was considered statistically significant and supports rejection of the null hypothesis. The null hypothesis states that there is no statistically significant difference in mean mineral content between the groups being studied. A 95% confidence interval was used for all statistical tests. Student's t-test results are reported in Table 5 for bulk mineralogy and in Table 6 for clay minerals.

.

Table 5 Student t-test results for bulk mineral X-ray diffraction data. Differences were considered statistically significant when the p-value was less than 0.05. A 95% confidence level was used for all tests.

Variable	Comparison	p-value
Calcite (%)	Aggregate vs 1-inch	8.69E-01
	Aggregate vs 2-inch	4.12E-01
	1-inch vs 2-inch	6.58E-01
Dolomite (%)	Aggregate vs 1-inch	7.56E-01
	Aggregate vs 2-inch	9.33E-01
	1-inch vs 2-inch	6.59E-01
Quartz (%)	Aggregate vs 1-inch	1.43E-01
	Aggregate vs 2-inch	2.52E-09
	1-inch vs 2-inch	7.80E-05

Table 6 Student t-test results for clay fraction X-ray diffraction data. Differences were considered statistically significant when the p-value was less than 0.05. A 95% confidence level was used for all tests.

Variable	Comparison	p-value
Illite (%)	Aggregate vs 1-inch	4.33E-01
	Aggregate vs 2-inch	9.51E-04
	1-inch vs 2-inch	8.31E-04
Chlorite (%)	Aggregate vs 1-inch	3.00E-01
	Aggregate vs 2-inch	4.73E-06
	1-inch vs 2-inch	4.17E-05
Kaolinite (%)	Aggregate vs 1-inch	3.51E-01
	Aggregate vs 2-inch	4.11E-02
	1-inch vs 2-inch	1.02E-02
Smectite (%)	Aggregate vs 1-inch	6.89E-01
	Aggregate vs 2-inch	1.51E-02
	1-inch vs 2-inch	1.02E-02

Our results show that no statistically significant differences were found between aggregates and 1-inch cores for any bulk or clay mineral (all p-values > 0.05). For bulk minerals, calcite and dolomite contents were consistent across all sample sizes, with no statistically significant differences for any comparison. For calcite, the smallest p-value was 0.41, and for dolomite, the minimum p-value was 0.67. In contrast, average quartz content decreased with increasing size. Statistically significant differences were observed for aggregates vs. 2-inch cores, with a p-value = 2.52×10^{-9} and for 1-inch vs. 2-inch with a p-value = 7.8×10^{-5}. The null hypothesis was rejected for both comparisons.

Among the clay minerals, several showed statistical significance between sample scales. Chlorite content was significantly different with p-value = 4.73×10^{-6} for aggregates vs. 2-inch cores, and with p-value = 4.17×10^{-5} for 1-inch vs. 2-inch cores. The null hypothesis was rejected in both comparisons. Kaolinite also showed significant differences, with p-value =0.04 for aggregates vs. 2-inch cores and p-value = 0.01 for 1-inch vs. 2-inch cores. The null hypothesis was rejected for both comparisons. Illite and smectite generally increased from aggregates to 2-inch samples. Illite showed statistically significant differences, with p-value = 9.51×10^{-4} for aggregates vs. 2-inch cores and p-value = 8.31×10^{-4} for 1-inch vs. 2-inch cores. Smectite showed statistically significant differences, with p-value = 0.02 for aggregates vs. 2-inch cores and p-value = 0.01 for 1-inch vs. 2-inch cores. The null hypothesis was rejected for both comparisons.

Overall, limestones are dominated by carbonate minerals, which correspond to the consistent and stable quantities of calcite and dolomite found in these samples. Rather than the main carbonate phases, the observed scale-related differences are likely driven by minor heterogeneity and sampling methods, which may obscure trends. Although present in low concentrations (< 4.5%), quartz was the only bulk mineral that showed statistical significance with size, suggesting that even small amounts may contribute to scale-related variation. Smaller specimens are more likely to represent a single, localized lithology or a specific small-scale feature, such as a quartz vein or localized clay patches. On the other hand, a large sample size may average out rock properties and composition. According to MacDonald et al. (2009), heterogeneity arises from many sources, including sedimentary fabrics, depositional environments, depositional cyclicity, diagenesis, fracturing, and faulting. Among these, diagenesis was identified as a major contributing factor to heterogeneity in carbonates. These processes may contribute to compositional heterogeneity at scales ranging from the reservoir scale to the pore scale (MacDonald et al., 2009).

Additionally, the sampling methods used may also influence the observed trends. The bulk mineralogy procedure requires mounting only a few milligrams of the powdered sample onto a zero-background plate, while clay fraction analysis uses approximately 15 grams of coarse rock. In both cases, only a portion of the sample material is analyzed. Although attempts were made to sample from representative zones, the small amounts used may not fully capture the compositional variation and heterogeneity of the limestone samples. Moreover, semiquantitative clay XRD measures the relative proportions of clay phases within the clay fraction. Therefore, the results reflect relative clay mineral composition and do not reflect the total clay content or weight percentage of clay minerals in the bulk sample. Furthermore, bulk and clay XRD analyses for aggregates and 1-inch cores were conducted in a separate laboratory from the 2-inch core analyses, which may contribute to the observed differences.

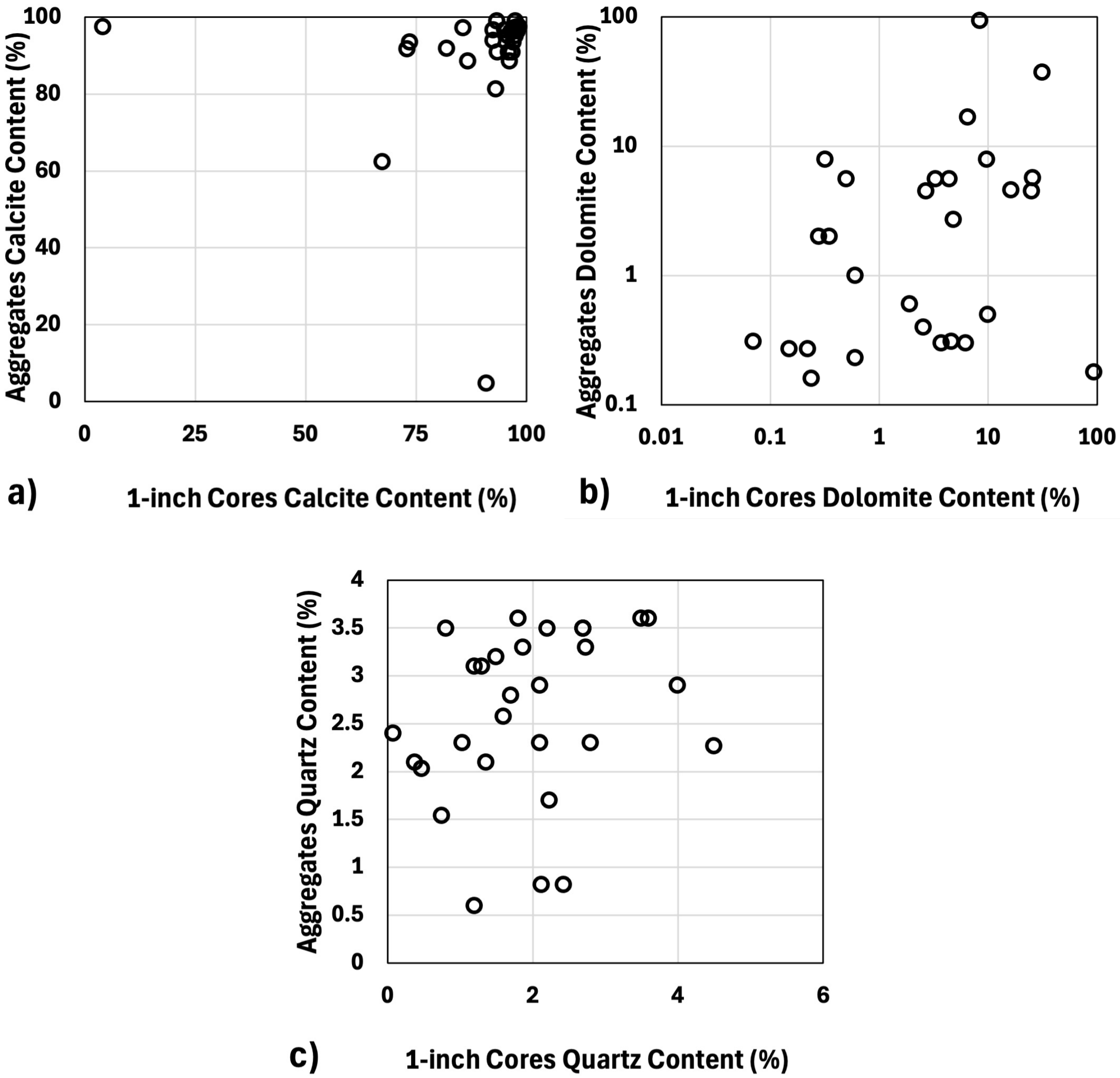

Figure 3.10 Comparison of bulk mineralogy between aggregate and 1-inch core samples for (a) calcite, (b) dolomite, and (c) quartz content (%).

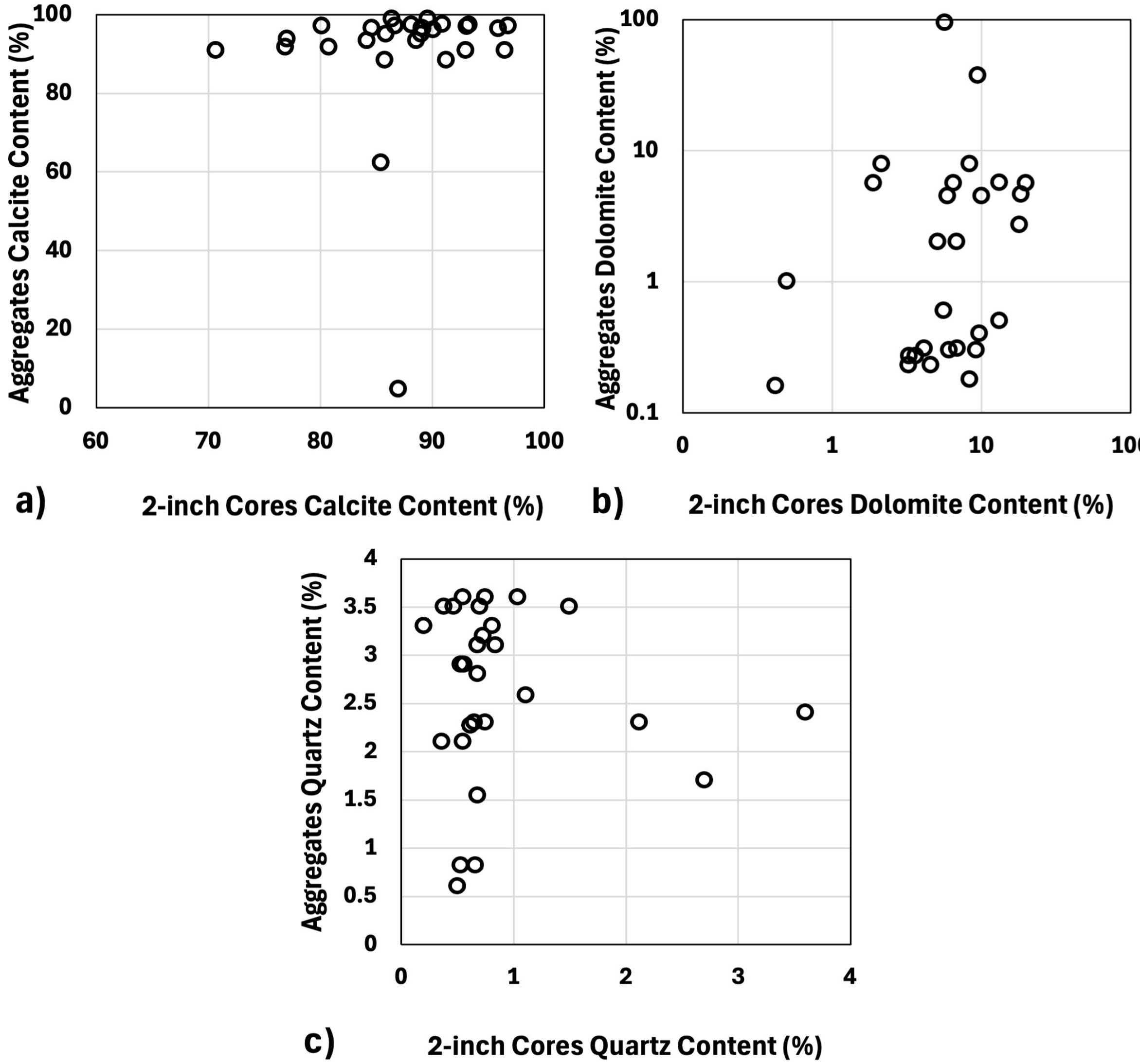

Figure 3.11 Comparison of bulk mineralogy between aggregate and 2-inch core samples for (a) calcite, (b) dolomite, and (c) quartz content (%).

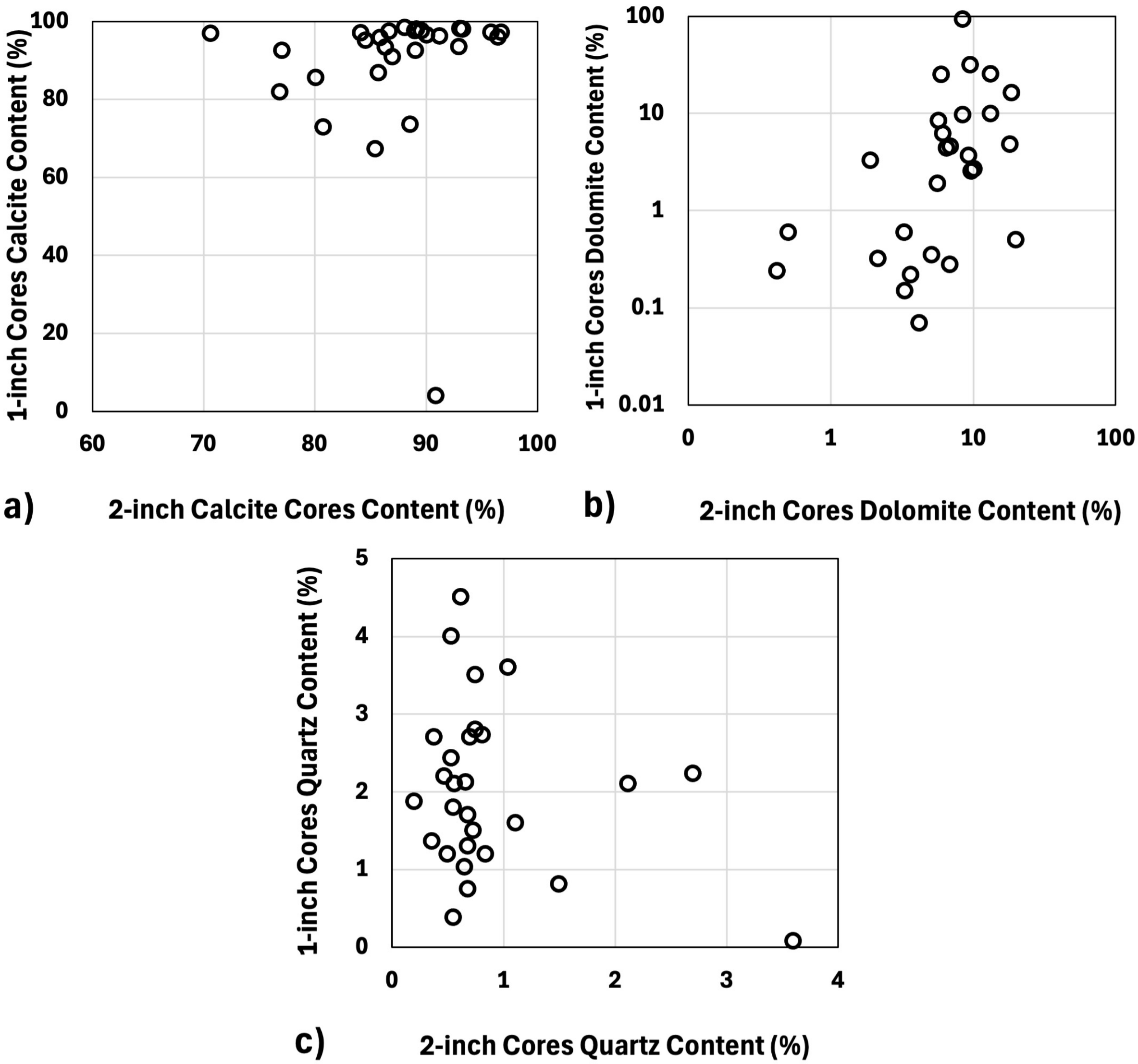

Figure 3.12 Comparison of bulk mineralogy between 1-inch and 2-inch core samples for (a) calcite, (b) dolomite, and (c) quartz content (%).

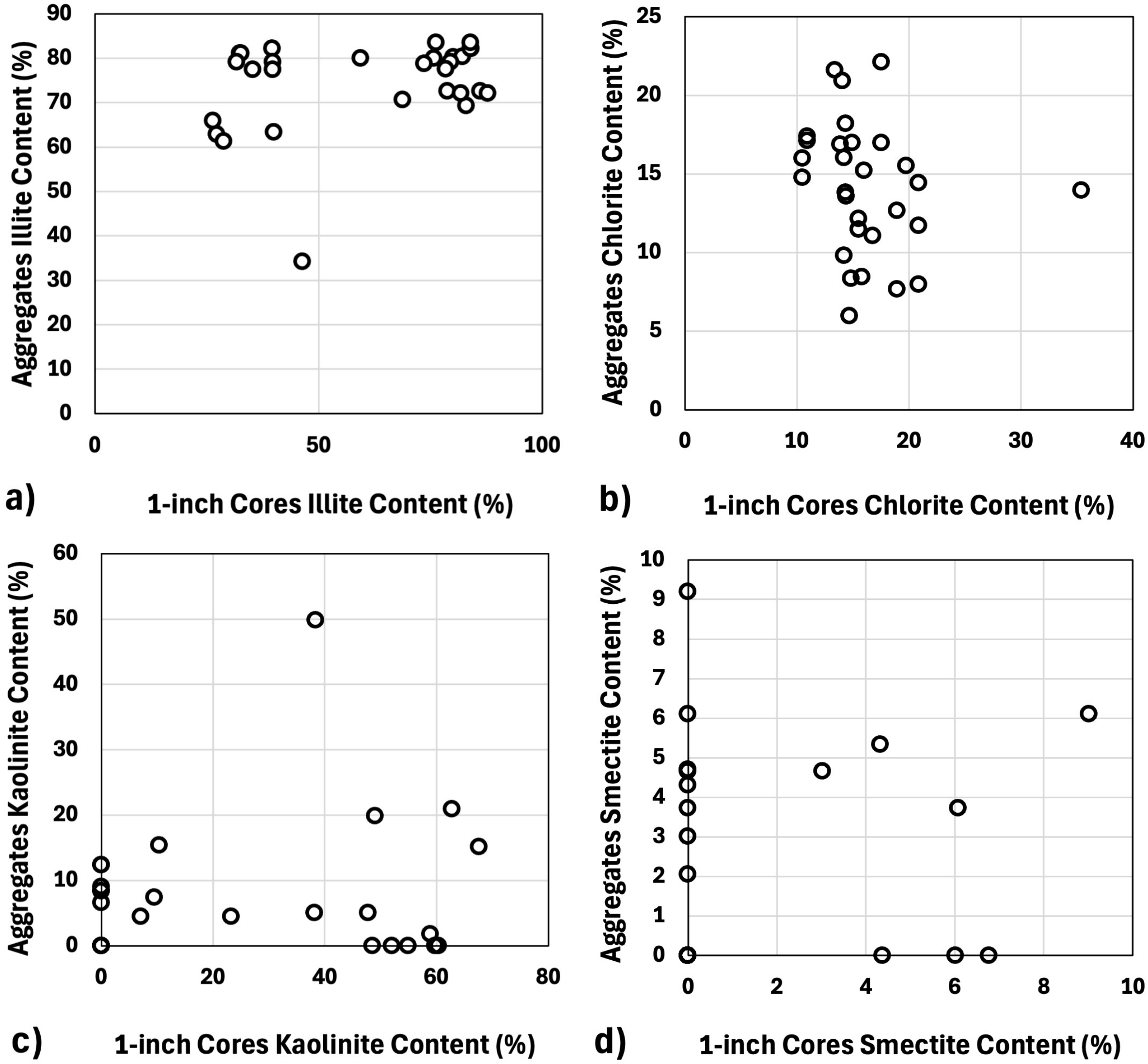

Figure 3.13 Comparison of clay fraction (<2 μm) mineralogy between aggregate and 1-inch core samples for (a) illite, (b) chlorite, (c) kaolinite, and (d) smectite content (%).

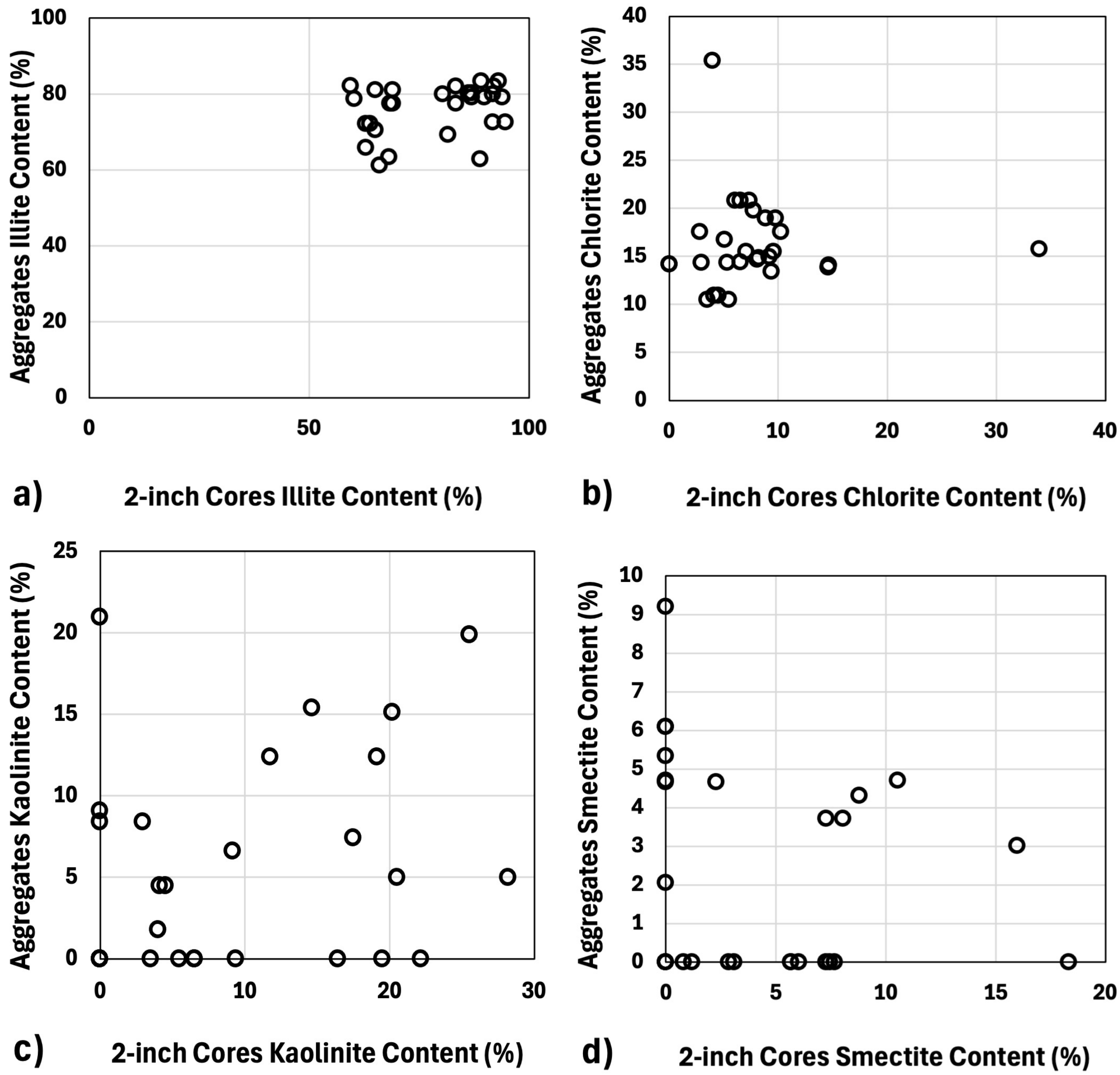

Figure 3.14 Comparison of clay fraction (<2 µm) mineralogy between aggregate and 2-inch core samples for (a) illite, (b) chlorite, (c) kaolinite, and (d) smectite content (%).

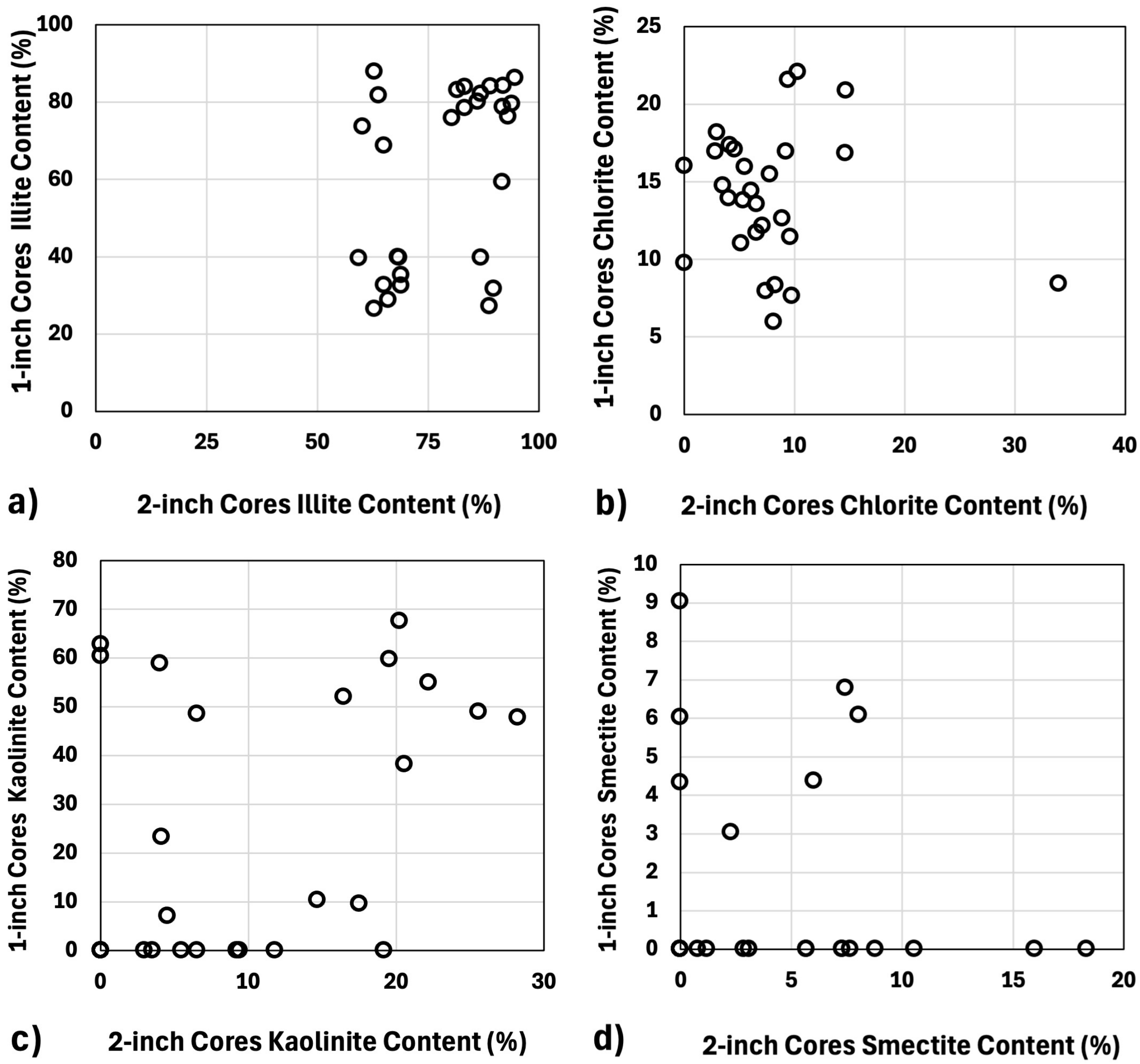

Figure 3.15 Comparison of clay fraction (<2 µm) mineralogy between 1-inch and 2-inch core samples for (a) illite, (b) chlorite, (c) kaolinite, and (d) smectite content (%).

3.3.2 Young's Modulus Scale Effects

To assess the effect of size on E, we compared 1-inch and 2-inch cores with a fixed 1-inch diameter, under both dry and wet conditions (Figure 22). Because only the length differed, the 2-inch cores had twice the volume of the 1-inch cores, and the length-to-diameter (L/D) ratio increased from 1.0 in 1-inch samples, to 2.0 for the 2-inch samples.

Student t-test with unequal variances was conducted to evaluate whether *E* differed between 1-inch and 2-inch cores. Student t-test were performed on the entire dataset and conducted separately for dry and wet groups. A p-value < 0.05 was considered a statistically significant difference in *E* between groups and supports rejecting the null hypothesis, whereas a p-value > 0.05 suggests that the difference is not statistically significant and fails to reject the null hypothesis. For every test, the null hypothesis states that there is no significant difference in *E* between the groups being tested. A 95% confidence level was used for all statistical tests.

For wet and dry cores combined, the difference in mean *E* between 1-inch cores (28.9 GPa) and 2-inch cores (25.2 GPa) was not statistically significant, based on p-value = 0.24 (> 0.05). For dry conditions, 1-inch cores had a slightly higher average *E* (30.4 GPa) compared to 2-inch cores (29.3 GPa), however, the difference in *E* between sizes was not statistically significant, with p-value = 0.8 (> 0.05). Similarly, in wet conditions, 1-inch cores had a higher *E* (27.3 GPa) compared to 2-inch cores (21.6 GPa). However, the difference was not statistically significant, with p-value = 0.21 (> 0.05). Across all conditions, *E* showed no consistent trend with core length, indicating no scale dependence within this L/D ratio range.

The L/D ratio is a key factor in uniaxial compression testing that affects stress distribution, failure mode, and mechanical behavior under static loading (Peng et al., 2025). Some prior studies have reported increases in *E* as the L/D of samples increases. For example, Li et al. (2021) found that when the L/D ratio changed from 1 to 6.7 in sandstone, *E* increased slightly, varying by -5% to +23%. Al-Rkaby and Alafandi (2015) observed that *E* was lowest at L/D =1 and increased when the ratio deviated above or below this value. Dai et al. (2020) found a logarithmic increase in sandstone *E* from 37.9 to 71 GPa as L/D increased from 0.5 to 3.0, with a transition in failure mode at L/D = 1.5. They found that the greater the slenderness ratio, the larger the *E.* Similarly, Sujatono (2024) reported a strong correlation (R = 0.98) between L/D and *E* for floatstone, with moduli increasing by 45.9 MPa per 1% L/D increase and stabilizing near 2.2. They identified this ratio as optimal, as changes before this point were rapid while changes after this ratio were less significant. Moreover, ASTM recommends a L/D ratio of 2.0-2.5 to obtain reliable and representable measurements.

In contrast, our results showed no consistent relationship between core length and *E*, suggesting that *E* is independent of core length within this range. This may reflect the narrow range of specimen sizes tested in our study. In accordance with our results, studies have also reported no relationship with scale. For instance, Olsen et al. (2008) found no variation in *E* with sample length in chalk, regardless of whether strain gages or linear variable differential transformers were used for measurements. Similarly, Tuncay et al. (2023) found no universal relationship between L/D and *E* in measurements based on 884 rock samples spanning multiple lithologies with L/D ratios from 1 to 3. In addition, Aghajanzadeh et al. (2025) observed an opposite effect where *E* increased from 1.8 to 5.6 GPa as the L/D decreased from 4.0 to 0.5 in shaley sandstones. They attributed this trend to stress distribution effects, where higher L/D samples exhibited more uniform axial loading and lower L/D samples experienced greater stress concentration near the ends.

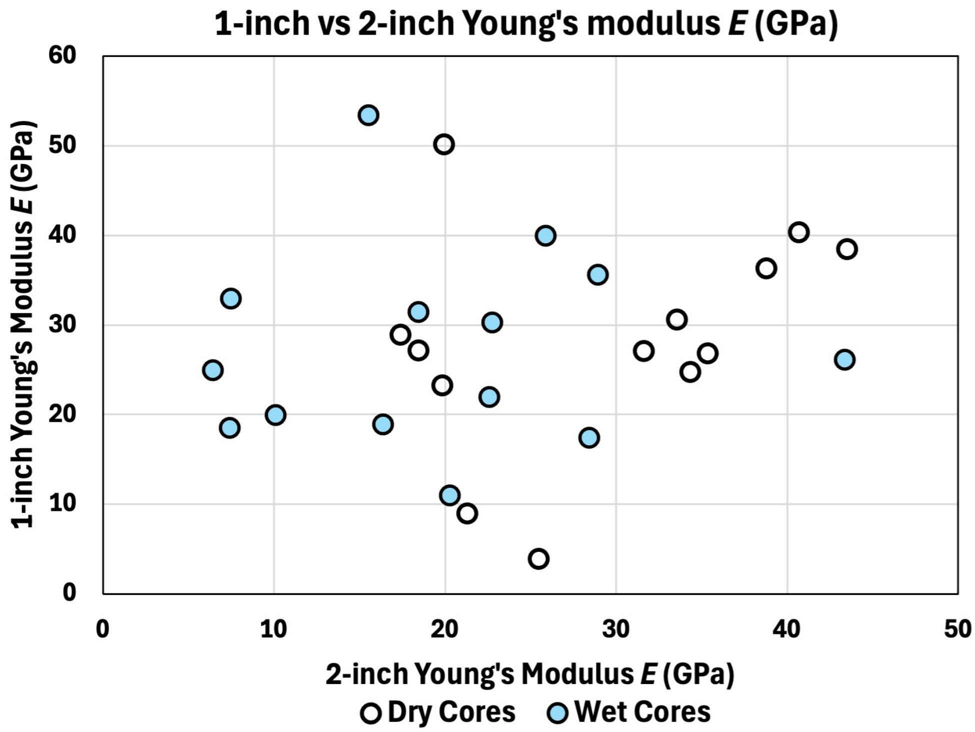

Figure 3.16 1-inch vs. 2-inch Young's modulus *E* for wet and dry core samples. Blue-filled circles represent wet samples, and unfilled circles represent dry samples. Based on the paired Student t-test, we found p-value = 0.8 (> 0.05; no significant difference).

3.4 Limitations

While this study evaluated two different core lengths, the range did not capture significant scaling behavior. Future studies should consider a broad range of length-to-diameter ratios to more thoroughly evaluate the effects of length on *E*. Additionally, the adhesive and epoxy applied to the surface of core samples may locally increase stiffness or restrict water absorption, potentially influencing *E* and θ. The effect of these adhesives on *E* and θ was not studied and should be taken into consideration in future research. Core samples are also prone to surface irregularities and asymmetric leveling, which should be considered during testing. In our study, the small core size increased the risk of cracking, which limited the extent to which surfaces could be trimmed or ground flat. In addition, because core length was a controlled variable in this study, excess trimming could potentially compromise experimental consistency. As a result, uneven leveling could potentially influence stress distribution and contribute to variability in *E* measurements during uniaxial compression testing. Future studies may benefit from sample preparation and coring methods and should consider evaluating the effects of surface irregularities on *E* measurements.

Chapter 4 - Conclusions

This study demonstrates that θ exerts the most significant influence on the variability of *E* in wet limestone samples from Kansas, with saturation resulting in a decrease in *E*. However, the extent of *E* reduction varied across samples, reflecting complex interactions among θ, mineralogy, and intrinsic rock properties. This study presents a regression and decision tree-based model to estimate *E* from θ and quartz content in saturated limestone core samples. Contrary to our expectations based on the literature, bulk and clay mineralogical composition did not explain variability in *E*. Although statistically significant differences in quartz and clay mineral content were observed across various sample sizes, these differences did not explain the variability in *E*. Notably, *E* was not scale dependent within the tested size range. Overall, these findings suggest that estimations of the mechanical behavior of limestone are not solely based on mineralogy or saturation and should incorporate further multivariable approaches. Incorporating non-destructive testing and predictive modeling, such as machine learning models trained on multivariable datasets, could enhance the practical application and predictive power of *E* for evaluating aggregate materials.

References

Aboutaleb, S., Behnia, M., Bagherpour, R., & Bluekian, B. (2018). Using non-destructive tests for estimating uniaxial compressive strength and static Young's modulus of carbonate rocks via some modeling techniques. Bulletin of Engineering Geology and the Environment, 77(4), 1717-1728.

Al-Rkaby, A. H., & Alafandi, Z. M. (2015). Size effect on the unconfined compressive strength and Modulus of elasticity of limestone rock. Electronic Journal of Geotechnical Engineering, 20(12), 1393-1401

Aghajanzadeh, M., Li, D., Heidarpour, A., Bahaaddini, M., & Masoumi, H. (2025). Shape-Dependent Behavior of Intact Rock Under Creep Loading. Rock Mechanics and Rock Engineering, 58(4), 4225-4245.

Aquino, C., Inoue, M., Miura, H., Mizuta, M., & Okamoto, T. (2010). The effects of limestone aggregate on concrete properties. Construction and Building Materials, 24(12), 2363-2368.

ASTM Standard D7012 (2023). Standard test methods for compressive strength and elastic moduli of intact rock core specimens under varying states of stress and temperatures. ASTM International, West Conshohocken, PA. DOI:10.1520/D7012-10, www.astm.org.

Breiman, L., Friedman, J., Olshen, R. A., & Stone, C. J. (2017). Classification and regression trees. Chapman and Hall/CRC.

Cai, X., Zhou, Z., Liu, K., Du, X., & Zang, H. (2019). Water-weakening effects on the mechanical behavior of different rock types: phenomena and mechanisms. Applied Sciences, 9(20), 4450.

Chen, F., Sun, X., & Lu, H. (2022). Influence of water content on the mechanical characteristics of mudstone with high smectite content. *Geofluids*, *2022*(1), 9855213.

Chen, Z. L., Shi, H. Z., Xiong, C., He, W. H., Wang, H. Z., Wang, B., ... & Ge, K. Q. (2023). Effects of mineralogical composition on uniaxial compressive strengths of sedimentary rocks. *Petroleum Science*, *20*(5), 3062-3073.

Dai, B., Zhao, X., Zhang, S., Kang, Q., & Zhu, Z. (2020). Mechanical behavior and energy evolution of sandstone considering slenderness ratio effect. Advances in Civil Engineering, 2020(1), 8881416.

Daraei, A., & Zare, S. (2018). Determination of critical saturation degree in rocks based on maximum loss of uniaxial compression strength and deformation modulus. Geomechanics and Geophysics for Geo-Energy and Geo-Resources, 4(4), 343-353.

Doebelin, N., & Kleeberg, R. (2015). Profex: a graphical user interface for the Rietveld refinement program BGMN. Journal of applied crystallography, 48(5), 1573-1580.

Erguler, Z. A., & Ulusay, R. (2009). Water-induced variations in mechanical properties of clay-bearing rocks. International Journal of Rock Mechanics and Mining Sciences, 46(2), 355-370.

Ermrich, M., & Opper, D. (2013). XRD for the analyst. Getting acquainted with the principles. Second. Panalytical.

Flügel, E. (2012). Microfacies analysis of limestones. Springer Science & Business Media.

Ghafoori, M., Rastegarnia, A., & Lashkaripour, G. R. (2018). Estimation of static parameters based on dynamical and physical properties in limestone rocks. Journal of African Earth Sciences, 137, 22-31.

Hadi, F., & Nygaard, R. (2023). Estimating unconfined compressive strength and Young's modulus of carbonate rocks from petrophysical properties. Petroleum Science and Technology, 41(13), 1367-1389.

Karakus, M., Kumral, M., & Kilic, O. (2005). Predicting elastic properties of intact rocks from index tests using multiple regression modelling. International Journal of Rock Mechanics and Mining Sciences, 42(2), 323-330.

Kim, E., Stine, M. A., & Martins de Oliveira, D. B. (2019). Effects of water content and loading rate on the mechanical properties of Berea Sandstone. Journal of the Southern African Institute of Mining and Metallurgy, 119(12), 1077-1082

Lashkaripour, G. R., Rastegarnia, A., & Ghafoori, M. (2018). Assessment of brittleness and empirical correlations between physical and mechanical parameters of the Asmari limestone in Khersan 2 dam site, in southwest of Iran. Journal of African Earth Sciences, 138, 124-132.

Li, H., Wang, J., Wang, X., Liang, W., Xu, G., & Kang, Y. (2022). Influence of water saturation time on microstructure and mechanical properties of jointed limestone. Frontiers in Earth Science, 10, 922683.

Li, H., Song, K., Tang, M., Qin, M., Liu, Z., Qu, M., ... & Li, Y. (2021). Determination of scale effects on mechanical properties of Berea Sandstone. Geofluids, 2021(1), 6637371.

Lin, S., & Lai, B. (2013, September). Experimental investigation of water saturation effects on Barnett Shale's geomechanical behaviors. In SPE Annual Technical Conference and Exhibition? (p. D031S038R001). SPE.

Liu, Y., Cai, Y., Huang, S., Guo, Y., & Liu, G. (2020). Effect of water saturation on uniaxial compressive strength and damage degree of clay-bearing sandstone under freeze-thaw. Bulletin of Engineering Geology and the Environment, 79(4), 2021-2036.

Loh, W. Y. (2014). Fifty years of classification and regression trees. International Statistical Review, 82(3), 329-348.

Loh, W. Y. (2011). Classification and regression trees. Wiley interdisciplinary reviews: data mining and knowledge discovery, 1(1), 14-23.

MacDonald, R. M., Kersey, D. G., Zhang, T., Akbar, M., & Mousa, W. (2009, December). Effect of carbonate heterogeneity on core-log integration. In *SPE Kuwait International Petroleum Conference and Exhibition* (pp. SPE-127290). SPE.

Madhubabu, N., Singh, P. K., Kainthola, A., Mahanta, B., Tripathy, A., & Singh, T. N. (2016). Prediction of compressive strength and elastic modulus of carbonate rocks. Measurement, 88, 202-213.

Mondol, N. H., Jahren, J., Bjørlykke, K., & Brevik, I. (2008). Elastic properties of clay minerals. The Leading Edge, 27(6),

Moore, D. M., & Reynolds, R. J. (1989). X-ray Diffraction and the Identification and Analysis of Clay Minerals. Oxford University Press.

Moradian, Z. A., & Behnia, M. (2009). Predicting the uniaxial compressive strength and static Young's modulus of intact sedimentary rocks using the ultrasonic test. International Journal of Geomechanics, 9(1), 14-19.

Ng, K., & Santamarina, J. C. (2023). Mechanical and hydraulic properties of carbonate rock: The critical role of porosity. Journal of Rock Mechanics and Geotechnical Engineering, 15(4), 814–825. https://doi.org/10.1016/j.jrmge.2022.07.017

Olsen, C., Christensen, H. F., & Fabricius, I. L. (2008). Static and dynamic Young's moduli of chalk from the North Sea. Geophysics, 73(2), E41-E50.

Peng, K., Bai, Y., Luo, S., Luo, K., He, H., & Xi, Z. (2025). Influence of Length-to-Diameter Ratio on Static and Dynamic Behavior of Rocks: A Review and Perspective. Materials, 18(5), 1109.

Robbins, C. R., & Keller, W. D. (1952). Clay and other noncarbonate minerals in some limestones. Journal of Sedimentary Research, 22(3), 146-152.

Sujatono, S., & Wijaya, A. E. (2022). The influence of quartz content on modulus of elasticity and Poisson's ratio in quartz sandstone. Bulletin of Engineering Geology and the Environment, 81(7), 287.

Sujatono, S. (2024). Optimum length-to-diameter ratio of floatstone under uniaxial compressive strength test. Geotechnical and Geological Engineering, 42(3), 2045-2060

Supandi, S., Zakaria, Z., Sukiyah, E., & Sudradjat, A. (2019). The influence of kaolinite-illite toward mechanical properties of claystone. Open Geosciences, 11(1), 440-446

Steinberg, D. (2009). CART: classification and regression trees. In The top ten algorithms in data mining (pp. 193-216). Chapman and Hall/CRC

Tuncay, E., Özcan, N. T., & Kalender, A. (2019). An approach to predict the length-to-diameter ratio of a rock core specimen for uniaxial compression tests. Bulletin of Engineering Geology and the Environment, 78(7), 5467-5482.

U.S. Geological Survey. (2025). Mineral commodity summaries 2025 (Report No. 2025; Version 1.2, March 3, 2025; p. 212). U.S. Department of the Interior. https://doi.org/10.3133/mcs2025

Vafaie, A., & Kivi, I. R. (2020). An investigation on the effect of thermal maturity and rock composition on the mechanical behavior of carbonaceous shale formations. Marine and Petroleum Geology, 116, 104315.

Vásárhelyi, B. (2005). Technical note statistical analysis of the influence of water content on the strength of the Miocene limestone. Rock Mech Rock Eng, 38(1), 69-76.

Wang, S., Wu, Z., Chen, J., Liu, H., Wang, R., & Liu, J. (2022). Study of the effect of mineral components on the permeability impairment rate and stress sensitivity factor of shale. Geofluids, 2022(1), 4407252.

Wasantha, P. L. P., Ranjith, P. G., Permata, G., & Bing, D. (2018). Damage evolution and deformation behaviour of dry and saturated sandstones: insights gleaned from optical measurements. *Measurement*, *130*, 8-17.

Willett, J. C. (2023, January). Stone (crushed)1 - USGS Publications Warehouse. United States Geological Survey

Wong, L. N. Y., Maruvanchery, V., & Liu, G. (2016). Water effects on rock strength and stiffness degradation. Acta Geotechnica, 11, 713-7358d

Yale, D. P., & Jamieson, W. H. (1994, May). Static and dynamic rock mechanical properties in the Hugoton and Panoma fields, Kansas. In SPE Oklahoma City Oil and Gas Symposium/Production and Operations Symposium (pp. SPE-27939). SPE.

Yan, Y., Ding, W., Liu, G., & Wang, H. (2022). Effects of mineral crystal structure and properties on the macro-mechanical properties of rocks.

Zhang, X., Ren, M., Meng, Z., Zhang, B., & Li, J. (2021). Experimental study on the mechanical behavior of yunnan limestone in natural and saturated states. Advances in Civil Engineering, 2021, 1-16.

Zhang, Q., Liu, Y., He, G., Chen, Q., Ou, X., & Tian, J. (2023). Study on the effects of different water content rates on the strength and brittle plasticity of limestone. Applied Sciences, 13(8), 4685.

Appendix A -

Appendix Table A.1 Young's Modulus *E* measured under dry and wet conditions, with corresponding volumetric water content θ values for 1-inch and 2-inch core samples.

	1-inch Cores			2-inch Cores		
Sample No.	**Condition**	***E* (GPa)**	**θ (%)**	**Condition**	**E (GPa)**	**θ (%)**
1	Dry	26.8	0.0	Dry	35.4	0.0
2	Wet	25.0	9.0	-	-	-
3	Dry	27.1	0.0	-	-	-
4	Wet	18.9	8.7	-	-	-
5	Wet	21.9	17.1	Dry	18.5	0.0
7	Dry	9.0	0.0	Dry	21.3	0.0
9	Wet	32.9	13.0	Dry	33.6	0.0
10	-	-	-	Dry	25.5	0.0
11	Dry	30.6	0.0	Wet	19.9	17.2
12	Dry	3.9	-	-	-	-
14	-	-	-	Dry	34.4	0.0
15	Dry	23.2	0.0	-	-	-
16	-	-	-	Wet	31.6	10.3
17	Wet	30.3	5.7	Wet	38.8	15.4
19	Dry	24.7	0.0	-	-	-
20	-		-	Wet	40.7	18.7
23	Wet	18.5	15.7	-	-	-
24	-	-	-	Wet	17.4	6.9
25	Dry	27.1	0.0	-	-	-
26	-		-	Wet	20.0	10.9
27	Wet	35.6	6.7	-	-	-
28	-	-	-	Dry	43.6	0.0
29	Dry	36.3	0.0	-	-	-
30	-	-	-	Dry	6.5	0.0
32	-		-	Dry	16.4	0.0
33	Wet	11.0	8.7	-	-	-
34	-	-	-	Dry	22.6	0.0
35	Dry	40.3	0.0	Dry	7.5	0.0
36	Dry	28.9	0.0	Wet	22.8	4.0
37	Dry	50.1	0.0	Dry	7.4	0.0
38	Dry	38.5	0.0	Wet	29.0	4.9
39	Wet	26.1	6.5	Dry	20.3	0.0

40	Wet	53.4	3.6	Wet	43.4	5.1
41	Wet	31.5	7.1	Wet	15.5	11.4
42	Dry	40.7	0.0	Wet	18.5	9.5
43	Wet	17.4	5.5	Wet	28.5	8.1
44	Dry	48.1	0.0	Wet	10.1	5.6
45	Wet	20.0	8.8	Wet	25.9	8.2
46	Wet	40.0	1.4	Wet	50.0	1.0

Appendix Table A.2 Bulk rock mineral content (calcite, dolomite, quartz (%)) for ¾-inch limestone aggregates, with the corresponding uniaxial compression test condition (wet or dry) reported for each sample.

Aggregates				
Sample No.	Condition	Calcite (%)	Dolomite (%)	Quartz (%)
1	Dry	97.2	1.0	1.7
2	Dry	97.2	0.4	2.4
3	Dry	97.4	0.2	2.3
4	Dry	97.4	0.2	2.3
5	Dry	97.5	0.2	2.3
7	Dry	96.4	0.3	3.3
9	Dry	96.4	0.3	3.3
10	Dry	98.9	0.3	0.8
11	Dry	98.9	0.3	0.8
12	Dry	4.7	93.8	1.5
14	Dry	96.6	0.3	3.1
15	Dry	96.6	0.3	3.1
16	Dry	96.2	0.6	3.2
17	Dry	90.9	5.6	3.5
19	Dry	90.9	5.6	3.5
20	Dry	90.9	5.6	3.5
23	Dry	97.0	0.2	2.8
24	Dry	95.1	2.0	2.9
25	Dry	95.1	2.0	2.9
26	Dry	88.5	7.9	3.6
27	Dry	88.5	7.9	3.6
28	Dry	93.8	2.7	3.5
29	Dry	97.2	0.5	2.3
30	Dry	91.8	4.6	3.6
32	Dry	93.4	4.5	2.1
33	Dry	93.4	4.5	2.1

34	Dry	91.7	5.7	2.6
35	Dry	62.3	37.1	0.6
36	Dry	81.2	16.8	2.0
37	Dry	96.6	1.0	2.4
38	Dry	91.5	6.1	2.3
39	Dry	75.3	23.3	1.4
40	Dry	83.4	15.5	1.1
41	Dry	92.3	7.2	0.5
42	Dry	94.1	4.9	1.1
43	Dry	93.3	4.9	1.8
44	Dry	92.8	5.1	2.2
45	Dry	74.8	23.2	2.0
46	Dry	89.5	0.1	0.8

Appendix Table A.3 Bulk rock mineral content (calcite, dolomite, quartz (%)) for 1-inch limestone cores and the corresponding uniaxial compression test condition (wet or dry).

1-inch Cores				
Sample No.	**Condition**	**Calcite (%)**	**Dolomite (%)**	**Quartz (%)**
1	Dry	97.2	0.6	2.2
2	Wet	96.8	0.5	2.7
3	Dry	97.4	2.6	0.1
4	Wet	98.1	0.2	1.7
5	Wet	97.5	0.4	2.1
7	Dry	97.9	0.0	2.1
9	Wet	95.8	0.3	4.0
11	Dry	98.3	0.6	1.0
12	Dry	4.0	93.3	2.8
15	Dry	97.1	0.2	2.7
17	Wet	86.7	9.7	3.6
19	Dry	97.9	0.2	1.9
23	Wet	96.2	0.3	3.5
25	Dry	93.3	4.6	2.1
27	Wet	92.5	4.8	2.7
29	Dry	97.5	0.1	2.4
33	Wet	85.6	9.9	4.5
35	Dry	90.9	8.4	0.8

36	Dry	92.5	6.2	1.3
37	Dry	95.1	3.7	1.2
38	Dry	96.5	1.9	1.5
39	Wet	81.9	16.3	1.8
40	Wet	97.0	2.7	0.4
41	Wet	73.5	25.1	1.4
42	Dry	95.9	3.3	0.8
43	Wet	72.9	25.5	1.6
44	Dry	93.4	4.4	2.2
45	Wet	67.3	31.5	1.2
46	Wet	93.0	6.5	0.5

Appendix Table A.4 Bulk rock mineral content (calcite, dolomite, quartz (%)) for 2-inch limestone cores, with the corresponding uniaxial compression test condition (wet or dry) reported for each sample.

2-inch Cores				
Sample No.	**Condition**	**Calcite (%)**	**Dolomite (%)**	**Quartz (%)**
1	Dry	93.3	0.9	3.1
5	Dry	93.3	0.9	3.1
7	Dry	93.5	0.2	3.0
9	Dry	88.1	3.3	3.8
10	Dry	93.5	1.0	2.0
11	Wet	93.9	0.8	2.2
14	Dry	93.6	0.5	3.0
16	Wet	92.2	0.9	3.2
17	Wet	70.7	19.9	4.4
20	Wet	93.1	0.4	3.0
24	Wet	89.0	5.1	3.3
26	Wet	85.9	6.8	3.5
28	Dry	89.2	3.6	4.6
30	Dry	86.4	6.9	3.3
32	Dry	89.6	4.2	3.5
34	Dry	87.0	5.7	4.2
35	Dry	89.1	6.1	2.0
36	Wet	85.8	8.4	1.8
37	Dry	84.6	9.3	3.0
38	Wet	91.2	2.1	2.9

39	Dry	90.1	5.6	1.7
40	Wet	77.1	18.0	1.9
41	Wet	80.1	13.2	2.5
42	Wet	76.9	18.5	1.9
43	Wet	84.2	10.1	3.0
44	Wet	88.6	6.0	2.8
45	Wet	80.8	13.3	2.0
46	Wet	85.5	9.5	1.8

Appendix Table A.5 Semi-quantitative clay fraction content (<2 µm) for aggregates samples, reporting chlorite, illite, kaolinite, and smectite content (%). The corresponding uniaxial compression test condition (wet or dry) is reported for each sample.

Aggregates					
Sample No.	**Condition**	**Chlorite (%)**	**Illite (%)**	**Kaolinite (%)**	**Smectite (%)**
1	Dry	19.8	80.2	0.0	0.0
2	Dry	14.4	80.2	0.0	5.3
3	Dry	14.2	82.1	0.0	3.7
4	Dry	14.2	82.1	0.0	3.7
5	Dry	15.0	69.2	6.6	9.2
7	Dry	14.4	72.5	8.4	4.7
9	Dry	14.4	72.5	8.4	4.7
10	Dry	11.0	79.9	4.5	4.7
11	Dry	11.0	79.9	4.5	4.7
12	Dry	35.4	62.8	1.8	0.0
14	Dry	19.0	81.0	0.0	0.0
15	Dry	19.0	81.0	0.0	0.0
16	Dry	14.9	82.1	0.0	3.0
17	Dry	20.9	79.1	0.0	0.0
19	Dry	20.9	79.1	0.0	0.0
20	Dry	20.9	79.1	0.0	0.0
23	Dry	13.4	77.5	9.1	0.0
24	Dry	10.5	83.4	0.0	6.1
25	Dry	10.5	83.4	0.0	6.1
26	Dry	15.5	72.1	12.4	0.0
27	Dry	15.5	72.1	12.4	0.0
28	Dry	13.9	78.7	7.4	0.0
29	Dry	14.1	70.5	15.4	0.0

30	Dry	16.8	63.3	19.9	0.0
32	Dry	17.6	77.4	5.0	0.0
33	Dry	17.6	77.4	5.0	0.0
34	Dry	14.7	65.9	15.1	4.3
35	Dry	15.8	61.2	20.9	2.1
36	Dry	16.0	34.2	49.8	0.0
37	Dry	7.9	29.4	62.7	0.0
38	Dry	9.7	37.2	53.0	0.0
39	Dry	9.0	41.2	49.8	0.0
40	Dry	35.6	55.6	8.8	0.0
41	Dry	7.0	29.3	63.7	0.0
42	Dry	13.2	37.8	49.0	0.0
43	Dry	12.6	31.7	54.8	0.9
44	Dry	6.2	24.1	69.7	0.0
45	Dry	12.2	37.9	49.9	0.0
46	Dry	15.2	49.4	35.5	0.0

Appendix Table A.6 Semi-quantitative clay fraction content (<2 µm) of 1-inch limestone core samples, reporting chlorite, illite, kaolinite, and smectite content (%). The corresponding uniaxial compression test condition (wet or dry) is reported for each sample.

1-inch Cores					
Sample No.	**Condition**	**Chlorite (%)**	**Illite (%)**	**Kaolinite (%)**	**Smectite (%)**
1	Dry	15.5	80.1	0.0	4.4
2	Wet	14.4	79.6	0.0	6.0
3	Dry	13.6	82.1	0.0	4.3
4	Wet	21.6	78.4	0.0	0.0
5	Wet	14.8	76.2	0.0	9.0
7	Dry	9.8	84.1	0.0	6.1
9	Wet	16.0	84.0	0.0	0.0
11	Dry	16.0	84.0	0.0	0.0
12	Dry	17.0	83.0	0.0	0.0
15	Dry	18.2	78.8	0.0	3.0
17	Wet	12.2	87.8	0.0	0.0
19	Dry	13.8	86.2	0.0	0.0
23	Wet	11.5	81.8	0.0	6.8
25	Dry	17.4	59.3	23.3	0.0

27	Wet	16.9	73.6	9.5	0.0
29	Dry	17.1	75.8	7.1	0.0
33	Wet	20.9	68.8	10.3	0.0
35	Dry	13.9	27.2	58.9	0.0
36	Dry	12.7	32.4	54.9	0.0
37	Dry	7.6	32.6	59.7	0.0
38	Dry	8.3	39.6	52.0	0.0
39	Wet	11.1	39.9	49.0	0.0
40	Wet	22.1	39.7	38.2	0.0
41	Wet	17.0	35.3	47.8	0.0
42	Dry	11.7	39.7	48.6	0.0
43	Wet	6.0	26.4	67.6	0.0
44	Dry	8.0	31.7	60.4	0.0
45	Wet	8.4	28.8	62.8	0.0
46	Wet	15.2	46.4	38.4	0.0

Appendix Table A.7 Semi-quantitative clay fraction content (<2 µm) in 2-inch limestone core samples, reporting chlorite, illite, kaolinite, and smectite content (%). The corresponding uniaxial compression test condition (wet or dry) is noted for each sample.

2-inch Cores					
Sample No.	**Condition**	**Chlorite (%)**	**Illite (%)**	**Kaolinite (%)**	**Smectite (%)**
1	Dry	7.8	86.2	0.0	6.0
5	Dry	6.5	87.0	6.5	0.0
7	Dry	0.0	92.0	0.0	8.0
9	Dry	0.0	83.3	9.4	7.3
10	Dry	9.2	81.6	9.2	0.0
11	Wet	6.5	87.0	6.5	0.0
14	Dry	3.0	91.8	3.0	2.3
16	Wet	7.3	89.8	0.0	2.9
17	Wet	6.0	94.0	0.0	0.0
20	Wet	9.4	83.3	0.0	7.3
24	Wet	3.5	93.0	3.5	0.0
26	Wet	5.5	89.1	5.5	0.0

28	Dry	5.3	94.7	0.0	0.0
30	Dry	4.1	91.7	4.1	0.0
32	Dry	4.5	80.4	4.5	10.6
34	Dry	4.0	88.9	4.0	3.1
35	Dry	8.9	69.0	22.2	0.0
36	Wet	7.1	62.8	11.8	18.3
37	Dry	9.8	65.0	19.5	5.7
38	Wet	9.6	63.8	19.1	7.4
39	Dry	8.2	59.4	16.4	16.0
40	Wet	14.6	60.3	17.5	7.7
41	Wet	14.6	65.0	14.6	5.7
42	Wet	5.1	68.1	25.6	1.2
43	Wet	10.3	68.4	20.5	0.8
44	Wet	2.8	69.0	28.2	0.0
45	Wet	8.1	62.9	20.2	8.8
46	Wet	34.0	66.0	0.0	0.0